DENISON QUEIROZ POGORZELSKI

MULTI-REACTIONAL KINETIC MODELING OF PHOSPHATE SORPTION ON GOETHITE USING ARTIFICIAL NEURAL NETWORKS

Thesis submitted to the Soil and Plant Nutrition Graduate Program of the Universidade Federal de Viçosa in fulfillment of the requirements for the degree of *Doctor Scientiae*.

Adviser: Leonardus Vergütz

Co-advisers: Emílio Borges
Edson Márcio Mattiello

VIÇOSA - MINAS GERAIS
2021

Ficha catalográfica elaborada pela Biblioteca Central da Universidade Federal de Viçosa - Campus Viçosa

T
P746m
2021

Pogorzelski, Denison Queiroz, 1986-
Multi-reactional kinetic modeling of phosphate sorption on goethite using artificial neural networks / Denison Queiroz Pogorzelski. – Viçosa, MG, 2021.
1 tese eletrônica (45 f.): il. (algumas color.).

Texto em inglês.
Inclui anexo.
Orientador: Leonardus Vergütz.
Tese (doutorado) - Universidade Federal de Viçosa, Departamento de Solos, 2021.
Referências bibliográficas: f. 37-45.
DOI: https://doi.org/10.47328/ufvbbt.2021.120
Modo de acesso: World Wide Web.

1. Fosfatos - Absorção e adsorção. 2. Dessorção. 3. Hopfield, Modelo de. 4. Redes neurais (Computação). I. Vergütz, Leonardus, 1982-. II. Universidade Federal de Viçosa. Departamento de Solos. Programa de Pós-Graduação em Solos e Nutrição de Plantas. III. Título.

CDD 22. ed. 631.43

Bibliotecário(a) responsável: Alice Regina Pinto CRB6 2523

DENISON QUEIROZ POGORZELSKI

MULTI-REACTIONAL KINETIC MODELING OF PHOSPHATE SORPTION ON GOETHITE USING ARTIFICIAL NEURAL NETWORKS

Thesis submitted to the Soil Science and Plant Nutrition Graduate Program of the Universidade Federal de Viçosa in fulfillment of the requirements for the degree of *Doctor Scientiae*.

APPROVED: June 28, 2021.

Assent:

Denison Q.

Denison Queiroz Pogorzelski
Author

Leonardus Vergütz
Adviser

To Vanúcia Schumacher and Kurt Schumacher Pogorzelski

ACKNOWLEDGEMENTS

To the Ministério da Educação (MEC - Brasil) of yore. I am grateful to the Sistema Unificado de Seleção - SiSU that allowed me to access to the university. That and other public policies have allowed the children of janitors, domestic workers, farmers and other people to have access to the university. So, I thank the Brazilian society for the investment in my education.

To the Federal University of Viçosa (UFV), for the opportunity to complete the postgraduate course.

To the Conselho Nacional de Desenvolvimento Científico e Tecnológico (CNPq), for granting the scholarship.

To the CAPES because this study was financed in part by the Coordenação de Aperfeiçoamento de Pessoal de Nível Superior – Brasil (CAPES) – Finance Code 001.

To the friends who received me at UFV (colleagues, lab technicians, professors and other administrators).

I thank my parents for encouraging education and hard work. These incentives were not said, but demonstrated through practical examples.

I thank my family for emotional support, especially my wife and son.

BIOGRAPHY

DENISON QUEIROZ POGORZELSKI, son of Joaquim Pogorzelski (farmer) and Marlete Queiroz Pogorzelski (farmer and teacher), was born in Camaquã-RS on April 22, 1986. In March 2010, he joined the Federal University of Pelotas (UFPel), Pelotas - RS, to study Agronomy, graduating in January 2015. In March 2015 he started his master's degree in the Graduate Program in Soil Science and Plant Nutrition at the Federal University of Viçosa (UFV), Viçosa-MG, under guidance Prof. Leônidas Carrijo de Azevedo Melo and Leonardus Vergütz, having defended his dissertation on February 24th, 2017. In March 2017, he joined the PhD Program in Soil Science and Plant Nutrition at UFV, having defended his thesis under the guidance of Prof. Leonardus Vergütz and co-supervision of Prof. Emílio Borges and Edson Márcio Mattiello.

ABSTRACT

POGORZELSKI, Denison, D.Sc., Universidade Federal de Viçosa, June, 2021. **Multi-reactional modeling of phosphate sorption on goethite using artificial neural networks**. Adviser: Leonardus Vergütz. Co-advisers: Emílio Borges and Edson Márcio Mattiello.

Phosphorus (P) is a limiting nutrient for plant biomass production in terrestrial ecosystems, and the nutrient raising the most concern regarding its use and availability. Most of this limitation occurs in the highly weathered soils of the tropics, where the low bioavailability and overall geochemical cycling of P are controlled by sorption reactions on soil minerals, especially oxides. Goethite is one of the most important Fe oxides present in these soils, with sorption reactions occurring at the goethite-water interface defining P fate in such environment. As such, understanding the mechanisms controlling P sorption on these materials is of uttermost importance to improve our overall understanding of the P biogeochemical cycling to improve P use efficiency. Herein, we are bringing an approach which consists in assessing P sorption and desorption capacity of goethite at different temperatures and then investigating the kinetic mechanisms by applying multi-reactional modeling through Hopfield artificial neural network (HANN). Two mechanisms were investigated, a sequential reactions type (P in solution $\rightleftharpoons$ B$\rightleftharpoons$ C) and another with independent reactions (B $\rightleftharpoons$ P in solution $\rightleftharpoons$ C). The mechanism that better fit the experimental data was used to provide the thermodynamic parameters. Furthermore, these mechanisms were also tested in a second sorption experiment on phosphate-preloaded goethite. The results showed that goethite adsorbed 13.34, 18.11 and 24.23 μmol g^{-1} of P and desorbed 48, 28 and 23 % of the sorbed P in water at 278, 298 and 323 K, respectively. After 20 days of incubation, phosphate-preloaded goethite sorbed 6.24 μmol g^{-1} more P and desorbed 54 % of that P at 298 K, demonstrating a lower adsorption capacity and a greater capacity for desorption facing a new P application. The mechanism with sequential steps better fit the experimental data, indicating that the step 1 (P in solution $\rightleftharpoons$ B) is the trigger for the step 2 (B $\rightleftharpoons$ C). Step 1 was faster than step 2, meaning that, kinetically, step 2 is the limiting step on P sorption mechanism onto goethite. Both steps were spontaneous ($\Delta G°<0$), but the step 1 was exothermic ($\Delta H°<0$) and an enthalpy driven reaction ($\Delta H°>T\Delta S°$), indicating that specie B is related to a high intermolecular interaction force with the goethite surface; while step 2 was endothermic ($\Delta H°>0$) and entropy driven ($\Delta H°<T\Delta S°$), indicating that specie C is related to surface or bulk precipitated Fe-P (e.g., strengite or an analogue). Both tested mechanisms failed

to fit the model on the P sorption data from second sorption experiment, indicating that the P sorption mechanism in phosphate-preloaded goethite has different key steps. This approach brings important information regarding P sorption on Fe oxides, one of the most important phenomena controlling P cycling and availability in highly weathered soils. Multi-reactional modeling by HANN were able to provide insights on the P sorption mechanism and their specific steps. Defining these steps and the thermodynamics controlling it help us clarifying and focusing our future research on our quest to elucidate such important environmental reactions.

Keywords: Stirred-flow system. P adsorption. P desorption. Rate constants. Hopfield artificial neural network.

RESUMO

POGORZELSKI, Denison, D.Sc., Universidade Federal de Viçosa, junho de 2021. **Modelagem multi-reacional de sorção de fosfato pela goethita usando redes neurais artificiais**. Orientador: Leonardus Vergütz. Coorientadores: Emílio Borges e Edson Márcio Mattiello.

O fósforo (P) é um nutriente limitante para a produção de biomassa vegetal em ecossistemas terrestres e o nutriente que mais preocupa quanto ao seu uso e disponibilidade. A maior parte dessa limitação ocorre em solos altamente intemperizados dos trópicos, onde a baixa biodisponibilidade e o ciclo geoquímico do P são controlados por reações de sorção em minerais do solo, principalmente os óxidos. Goethita é um dos mais importantes óxidos de Fe presentes nesses solos, com reações de sorção ocorrendo na interface goethita-água, definindo o destino do P nesse ambiente. Assim sendo, compreender os mecanismos que controlam a sorção de P nesses materiais é de extrema importância para melhorar nossa compreensão geral do ciclo biogeoquímico de P e assim melhorar a eficiência do uso de P. Para ajudar a resolver esse problema, estamos trazendo uma abordagem que consiste em avaliar a capacidade de sorção e dessorção de P da goethita-goethita previamente carregada com P em diferentes temperaturas e, em seguida, investigar os mecanismos cinéticos por meio da aplicação de modelagem multi-reacional através da rede neural artificial de Hopfield (RNAH). Dois mecanismos foram investigados, um tipo com reação sequencial (P em solução ⇌ B⇌ C) e outro com reações independentes (B ⇌ P em solução ⇌ C). O mecanismo que melhor se ajustou aos dados experimentais foi utilizado para fornecer os parâmetros termodinâmicos. Além disso, esses mecanismos também foram testados em um segundo experimento de sorção em goethita previamente carregada com fosfato. Os resultados mostraram que a goethita adsorveu 13,34, 18,11 e 24,23 μmol g^{-1} de P e dessorveu 48, 28 e 23% do P adsorvido em água a 278, 298 e 323 K, respectivamente. Após 20 dias de incubação, a goethita carregada com fosfato adsorveu 6,24 μmol g^{-1} a mais de P e dessorveu 54% desse P a 298 K, demonstrando menor capacidade de adsorção e maior capacidade de dessorção diante de uma nova aplicação de P. O mecanismo com etapas sequenciais se ajustou melhor aos dados experimentais, indicando que a etapa 1 (P na solução ⇌ B) é o gatilho para a etapa 2 (B ⇌ C). A etapa 1 foi mais rápida do que a etapa 2, o que significa que, cineticamente, a etapa 2 é a etapa limitante do mecanismo de sorção de P pela goethita. Ambas as etapas foram espontâneas (ΔG ° <0), mas a etapa 1 foi exotérmica (ΔH ° <0) e conduzida por entalpia (ΔH °> TΔS °), indicando que a espécie B apresenta uma

interação molecular forte com a superfície da goethita; enquanto a etapa 2 foi endotérmica (ΔH °> 0) e conduzida por entropia (ΔH ° <TΔS °), indicando que a espécie C está relacionada a precipitação de Fe-P em solução ou em superfície (e.g., estrangita ou um análogo). Ambos os mecanismos testados falharam em modelar os dados de sorção de P do segundo experimento de sorção, indicando que o mecanismo de sorção de P na goethita previamente carregada com fosfato tem mais de duas etapas chaves. Esta abordagem traz informações importantes sobre a sorção de P nos óxidos de Fe, um dos fenômenos mais importantes no controle da ciclagem e disponibilidade do P em solos altamente intemperizados. A modelagem multi-reacional por RNAH foi capaz de fornecer informações sobre o mecanismo de sorção de P e suas etapas específicas. Definir essas etapas e a termodinâmica que as controla nos ajuda a esclarecer e focar nossas pesquisas futuras em nossa busca para elucidar essas reações ambientais importantes.

Palavras-chave: Sistema de fluxo sob agitação. Adsorção de P. Dessorção de P. Constantes cinéticas. Rede neural artificial de Hopfield.

LIST OF ILLUSTRATIONS

LIST OF TABLES

SUMMARY

1 INTRODUCTION

Phosphorus (P) is a limiting nutrient for plant biomass production in terrestrial ecosystems, and the nutrient raising the most concern regarding its use and availability (Elser and Bennett, 2011). Most of this limitation occurs in the highly weathered soils of the tropics, where the low bioavailability and overall geochemical cycling of P are controlled by sorption reactions on soil minerals, especially oxides (Mendez et al., 2022).

Phosphate anions (e.g., $H_2PO_4^-$ and HPO_4^{2-}) represent the main form of P in the environment. The P concentration in the soil solution is governed by biological and physicochemical processes such as (im)mobilization by microbiota (Condron et al., 2015), P uptake by plants (Sahu et al., 2020; Vance et al., 2003), diffusion into soil aggregates (Saki et al., 2020), precipitation, and the adsorption at the solid-liquid interface of soil particles (Penn and Camberato, 2019). In highly weathered soils where the clay fraction minerals change from 2:1 silicates to kaolinite and oxides, the adsorption process of P becomes more important in controlling its fate and behavior in the environment (Eriksson et al., 2016; Wang et al., 2018). Therefore, understanding surface reactions is the key to move forward in studies of phosphate chemistry in soil (Barrow, 2015). Giving the difficulty to study surface reactions on soil samples due to their complexity in terms of mineralogy and organic compounds, pure soil minerals are used in the investigation of these reactions (Bowden et al., 1980; Gérard, 2016; Torrent, 1991; Torrent et al., 1990), including goethite (α-FeOOH), a representative mineral of tropical soils (Silva et al., 2020).

The P sorption on surface of soil minerals can be accessed by spectroscopic and chemical reactions-based approaches (e.g., kinetic)(Kruse et al., 2015). Spectroscopic studies elucidate the species that P assumes after interacting with the surface of soil minerals (Abdala et al., 2015a, 2015b; Arai and Sparks, 2001; Gustafsson et al., 2020; Li et al., 2013; Wang et al., 2018, 2019, 2017) and most of the recent efforts to understand P behavior in the soils have been done applying spectroscopic techniques. On the other hand, kinetic studies estimate the P mass transfer over time between the different species and brings thermodynamics information (Sun et al., 2019; Warrinnier et al., 2018). Through the rate constants, energetic parameters of the transition states can be estimated providing the energetics of the reactions that integrate the sorption mechanism and the thermodynamic stability of the products (Limousin, 2007; Liu, 2009; Nazari et al., 2006).

In general, kinetic approaches on P sorption mechanism are evaluated using closed systems (batch experiment), which show some limitations, including the difficulty of separating the solution from the solid phase in sufficient time to measure rapid initial reactions related to P adsorption (Eick et al., 1990); overestimating P adsorption capacity due to the precipitation of P in solution (Chen et

al., 1973); abrupt loading of P on mineral surface, unlike the gradual loading that occurs in the continuous-flow systems (Abdala et al., 2015a); and arduous procedure to measure P desorption (Penn and Warren, 2009). In contrast, stirred-flow systems (continuous-flow open systems) allow quick and easy access to the adsorption/desorption capacity of P; mitigate the cations excess into the reactor and therefore P precipitation in bulk solution, focusing on surface reactions; low and continuous loading of the surface; and easily simulates different experimental conditions, such as pH, ionic strength and concentrations of the target element (Bar-Tal et al., 1990; Eick et al., 1990; Fernández-Calviño et al., 2010; Guedes et al., 2016; Limousin, 2007; Pérez-Novo et al., 2011; Seyfried et al., 1989; Yin et al., 1997).

The kinetic modeling of the P sorption mechanism on soil minerals has been widely studied by empirical and phenomenological models (Barrow, 1983; Limousin, 2007; Warrinnier et al., 2018). Empirical models are restricted to describing kinetic behavior through parameters that do not explain the sorption mechanism. Usually, they only point to fast or slow stages of the kinetic profile and sorption capacity, but do not provide molecular information on the reactions that integrate the mechanism. On the other hand, phenomenological models can simulate the mechanisms controlling the reactions (multi-reactional models), which can happen consecutively or in parallel steps (Smolders et al., 2021; Sun et al., 2019; Sun and Selim, 2019). Consequently, multi-reactional models have many kinetic parameters related to the different species involved in the mechanism and, generally, the experimental concentration of a single species is monitored over time. Thereby, the challenge is to obtain the parameters and/or the kinetic model that originate this experimental concentration.

The kinetic treatment for this type of problem can be approached as an ill-posed inverse problem in which the kinetic parameters are obtained from experimental data related to concentrations of one or more species over time. The efficiency of a method based on artificial Hopfield neural networks for solving inverse problems in chemical kinetics has been reported (Tavares et al., 2020). Particularly, this algorithm proved to be more robust in the optimization of kinetic parameters than other recursive neural networks (Borges et al., 2012; Menezes et al., 2012). This algorithm has been applied to solve inverse problems in enzymatic chemical kinetics, hydrolysis reaction, calculations of molecular force field and potential energy surfaces (Borges et al., 2012; Lemes et al., 2008; Menezes et al., 2012; Sebastião et al., 2011). However, the methodology based on artificial Hopfield neural networks has not yet been used on the investigation of surface reactions, such as the mechanism of P sorption by minerals and minerals previously loaded with P.

In this sense, to fill the gap about the adsorption energetics of phosphate on goethite, we conducted herein temperature dependent stirred-flow studies on the adsorption of phosphate on goethite clay at pH 5. The experimental data was modeled by an artificial Hopfield neural network based on a two multi-reactional kinetic mechanism of P sorption onto goethite. This model provides insights on the steps of the mechanism, kinetic rates, activation energy barriers and the kinetically limiting step. Our goal is to improve our understanding of the geochemical cycling of P in tropical weathered soils, which should allow us to increase P use efficiency and help building more productive and sustainable agricultural systems.

2 MATERIAL AND METHODS

2.1 Sample preparation and characterization

Synthetic goethite (Fe 30-63 %, CAS 20344-49-4, Sigma-Aldrich) was added to deionized water, this suspension was stirred, centrifuged and the supernatant was discarded. This procedure was performed until the electric conductivity of the supernatant dropped below 35 $\mu S\ cm^{-1}$ (S70 SevenMulti conductivity meter) (Wang et al., 2019). The wet paste was oven dried at 309 K, then the goethite sample was crushed (mortar) and stored in desiccator to subsequently characterization.

The specific surface area (SSA, 35.53 $m^2\ g^{-1}$) of the goethite, its porous volume (PV, 0.033 $cm^3\ g^{-1}$) and size pore (SP, 18.31 Å) were obtained by N_2 physisorption (77.3 K, Quantachrome, NOVA 2200e). SSA was estimated by BET model (Brunauer et al., 1938) from multiple points of the isotherm sorption (multipoint approach) (Figure S1a). The PV and SP were estimated by BJH model (Barrett et al., 1951) from the multipoint approach (Figure S1b). The XRD analyses were performed in a Shimadzu XRD-6000 diffractometer, using a graphite crystal monochromator to select Co Kα radiation ($\lambda = 0.1789$ nm), and scanning rate of 0.02 ° $2\theta\ s^{-1}$ in the range from 5 to 70° 2θ (Figure S2). Furthermore, the morphology of the goethite crystals was observed by scanning electron microscopy (JEOL JSM-6010LA) (Figure S3). Briefly, the goethite showed acicular crystals with good crystallinity and low SSA.

2.2 Mineral suspension and background solutions

The pH of the goethite suspension (5 $g\ L^{-1}$) was adjusted over 20 days until equilibrium to pH 5 and was kept under constant agitation. The pH 5 is a fairly common pH for the weathered

tropical soils (dos Santos Teixeira et al., 2020) where goethite is commonly found. This pH is below the point of zero charge of Fe oxides like goethite found in the clay fraction of the soils (Fink, Jessé et al., 2016) and makes goethite mostly positively charged, as it is usually found in the soils.

For the P sorption/desorption experiments two solutions were used in the stirred-flow experiment: (i) a background solution without P (pH 5 and 10 mmol L^{-1} KCl, CAS 7447-040-7, Sigma-Aldrich) and (ii) a P solution (pH 5, 10 mmol L^{-1} KCl and 100 µmol L^{-1} P using KH_2PO_4, CAS 7778-77-0, Merck). The concentration of 10 mmol L^{-1} KCl was used to simulate the ionic strength of the soil solution (*e.g.*, Naidu et al., 1994). All pH adjustments were performed with HCl (10 mmol L^{-1}) or NaOH solution (10 mmol L^{-1}) (S70 SevenMulti of Mettler Toledo).

The low P concentration (100 µmol L^{-1}) was used in order to achieve a gradual loading of P on the mineral surface, mimicking natural soil conditions but also allowing us to follow the steps of this loading. On the other hand, the concentration of the goethite suspension (5 g L^{-1}) in the reactor was chosen to avoid its sedimentation during the experiment (homogeneous suspension). At the end, the chosen concentrations of P and goethite suspension allowed to access the kinetic profile of the P sorption reactions in a relatively short and feasible time (~74 min).

2.3 Stirred-flow experiment

Adsorption/desorption experiments in stirred-flow systems allow to access the kinetic profile of these reactions (Sun and Selim, 2019). Here we used a stirred-flow system with a flow rate of 1 mL min^{-1} to investigate the kinetic profile of P adsorption/desorption by goethite at three temperatures (278, 298 and 323 K ± 1 K). The system is comprised by the stock solution bottles (P containing solution or background no P solution), which are coupled to a multi-channel chromatographic pump that controls precisely the flow (1 mL min^{-1}) of the incoming solutions towards the small Teflon reactor (14 mL of internal capacity) where sorbent (goethite 5 g L^{-1}) is kept by a membrane filter (Fig. S4). The reactor is sitting on the top of a magnetic stirrer with temperature control that keeps the goethite in suspension and helps ensuring the desired temperature, aiding the water bath temperature control in which the stock solutions are placed. After the incoming solution passes through the reactor in contact with the sorbent, the entire solution is collected by a fraction collector to be analyzed afterwards. The fraction collector collects the solution for each 2 min (2 mL of solution) in 2.5 mL Eppendorf tubes during the 74 min of the adsorption phase and other 74 min of the desorption phase, which occur subsequently. The definition of this timing for the adsorption phase comes from the optimization of the system, when we defined that for the used P and goethite concentrations, we needed 74 min for the goethite to be completely loaded with P

and no further P adsorption would happen. For the desorption phase we kept the same timing as we also defined that it was enough to allow for the removal of most of the free and exchangeable P present in the system. Finally, these adsorption/desorption runs were carried out in duplicate and the results shown here are the average of these two runs.

The first step for the P adsorption/desorption experiments is to load the reactor (14 mL) with the previously adjusted pH 5 goethite suspension (5 g L^{-1}). After closing the reactor, the background solution (pH 5 and KCl 10 mmol L^{-1}) without P was injected in the reactor (1 mL min^{-1}) for 20 min to purge the system in order to remove air and stabilizing the pressure. After that, the background solution without P is switched to the P containing solution (pH 5, KCl 10 mmol L^{-1} and 100 µmol L^{-1} of P) and the P loading phase (adsorption phase) on the surface of goethite starts. After 74 min of this P containing solution passing through the reactor, goethite surface is completely loaded with P and no further P is adsorbed. At this point, the P containing solution is switched back to the background solution (pH 5 and KCl 10 mmol L^{-1}) without P and the desorbing phase starts, taking place for other 74 min.

During both adsorption and desorption phases we have a dilution effect inherently taking place. In order to account for this effect and to be able to calculate the adsorbed/desorbed P from goethite we perform the same procedures already explained for the adsorption and desorption phases, but without any goethite in the reactor (control). Throughout the text we call them “inert” curves. At the end, the P adsorption/desorption was estimated by the difference (gap) between the areas of the curves containing and non-containing goethite in the reactor (Limousin et al., 2007). Experimental data of the control (without goethite in the chamber) were close to those mathematically estimated for an ideal reactor, assuring us that the Limousin et al. (2007) method could be apply to the data treatment.

In order to improve our understanding regarding the P sorption mechanisms that takes place in the natural environment, a goethite suspension previously loaded with P (in equilibrium with 100 µmol L^{-1} of P at 298 K) was collected and hermetically stored at room temperature for 20 days. After that, the goethite suspension previously loaded with P was subjected to a new P sorption with the same P solution (pH 5, 10 mmol L^{-1} KCl and 100 µmol L^{-1} P). At the end, all the solution passing through the reactor and collected by the fraction collector had its P concentration quantified by the molybdenum blue method (Braga and Defelipo, 1974).

2.4 Sorption mechanisms and kinetic modeling: Numerical procedure

Assuming that the P sorption mechanism on soil minerals presents two steps (biphasic) and considering that the relationship between the steps can be sequentially dependent (Smolders et al., 2021) or not (Sun and Selim, 2019; Warrinnier et al., 2018), we tested two multi-reactional sorption mechanisms (Figure 1).

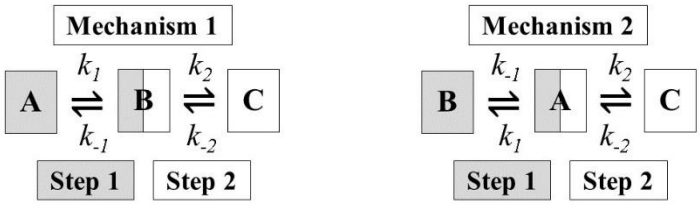

Figure 1. P sorption mechanisms with dependent (Mechanism 1) and independent steps (Mechanism 2), where A is the P in bulk solution and B and C are P sorbed partitions (P pools) (B+C = P sorbed).

The differential rate law for mechanisms 1 (Eq. 1-3) and 2 (Eq. 4-6) can be written as:

$$\frac{dA}{dt} = -k_1[A] + k_{-1}[B] \quad \text{Eq. 1}$$

$$\frac{dB}{dt} = k_1[A] - k_{-1}[B] - k_2[C] + k_{-2}[C] \quad \text{Eq. 2}$$

$$\frac{dC}{dt} = k_2[B] - k_{-2}[C] \quad \text{Eq. 3}$$

$$\frac{dB}{dt} = k_1[A] - k_{-1}[B] \quad \text{Eq. 4}$$

$$\frac{dA}{dt} = -k_1[A] + k_{-1}[B] - k_2[A] + k_{-2}[C] \quad \text{Eq. 5}$$

$$\frac{dC}{dt} = k_2[A] - k_{-2}[C] \quad \text{Eq. 6}$$

Where A is the P in the bulk solution (µmol L^{-1}) and B and C are species in equilibrium with bulk solution (µmol g^{-1} of P) and each other (µmol g^{-1} of P) at time (*t*). The parameters k_1, k_{-1}, k_2 and k_{-2} (s^{-1}) are the kinetic constants.

Based on the differential rate laws of the sorption mechanisms (Eq. 1-6), experimental data (consumption of P in solution) and an initial guess for the kinetic constants (Smolders et al., 2021), an ill-posed inverse problem was solved by a Hopfield artificial neural network (HANN) (Hopfield, 1984; Hopfield and Tank, 1985), which optimized the kinetic constants (Borges et al., 2012; Lemes et al., 2008; Menezes et al., 2012; Sebastião et al., 2011; Tavares et al., 2020).

A HANN presents neurons with a given state *u*. The neural states correspond to input information that is generated from an initial guess (kinetic constant - *u*). An activation function (Eq. 7) propagates the neural states through the network until a learning time τ reaches the optimization

criterion. This sigmoid activation function presents positive values for the output signals, being appropriate for obtaining positive parameters as kinetic constants.

$$f_i(\tau) = \frac{1}{2}[1 + \tanh(u_i)] \quad \text{Eq. 7}$$

The optimization criterion is defined by an error function (Eq. 8) based on difference between experimental (P_{exp}) and calculated vectors (P_{cal}) with n data.

$$E = \frac{1}{2}\sum_{j=1}^{n} e_j^2; \text{ where } e_j = P_{exp_j} - P_{cal_j} \quad \text{Eq. 8}$$

The error function depends on the neural state (u) to obtain the calculated vector ($P\ cal$), so this link is built in Eq. 9.

$$\frac{dE}{d\tau} = \sum_{i=1}^{n}\sum_{j=1}^{m}\left(e_j \frac{\partial P_{cal_j}}{\partial f_i}\frac{\partial f_i}{\partial u_i}\frac{\partial u_i}{\partial \tau}\right) \quad \text{Eq. 9}$$

where n is the quantity of neurons that correspond to the same number of investigated kinetic parameters, which in this study are four kinetic constants for both proposed mechanisms.

However, for the kinetic constants to be optimized (u), the output values of the error function need to decrease, *i.e.*, the error function should be minimized. Therefore, the condition of the Eq. 10 is applied in Eq. 9, resulting in the Eq. 11.

$$\frac{du_i}{d\tau} = -\sum_{i=1}^{n}\frac{\partial P_{cal_j}}{\partial f_i}\, e_j \quad \text{Eq. 10}$$

$$\frac{dE}{d\tau} = -\sum_{i=1}^{n}\frac{\partial f_i}{\partial u_i}\left(\frac{\partial u_i}{\partial \tau}\right)^2 \quad \text{Eq. 11}$$

The condition introduced by Eq. 10 (negative signal) and due to $\frac{\partial f_i}{\partial u_i} \geq 0$ and $e_j \geq 0$, guarantee that the derivative of the error with respect to learning time will be negative $\left(\frac{dE}{d\tau} < 0\right)$. When Eq. 8 reaches its lowest value, the kinetic constants are obtained (Figure 2). The algorithm for this numerical procedure was also described by Borges and Menezes (2017), Lemes et al. (2009 and 2008), Menezes et al. (2012) and Tavares et al. (2020).

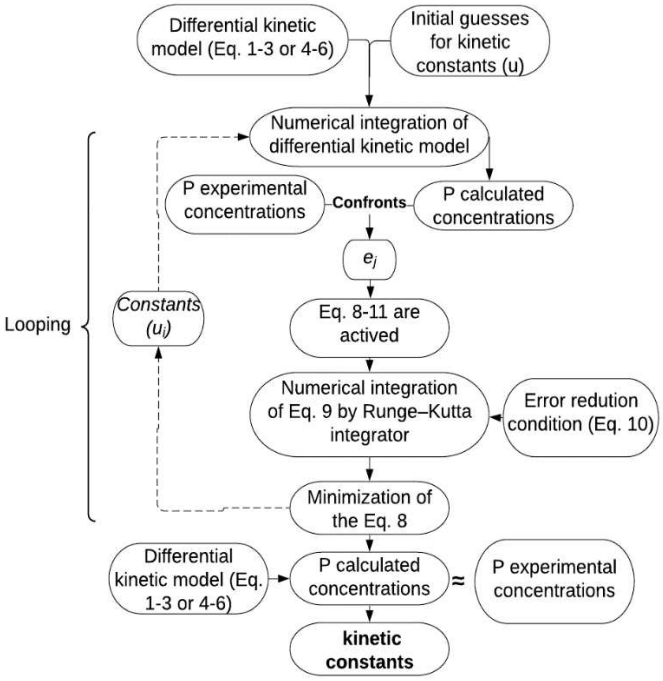

Figure 2. Hopfield neural network algorithm.

2.5 Thermodynamic parameters

The thermodynamic parameters of the kinetic steps of the best-fit mechanism were calculated. According to the transition-state theory (Eyring, 1935), the activation Gibbs free energy of the forward and backward steps of the mechanism could be obtained as follow (Menezes et al., 2012; Nazari et al., 2006):

$$\Delta G_1^{\ddagger^\circ} = -RT\ ln\left(\frac{k_1 h}{k_B T}\right) \quad \text{Eq. 12}$$

$$\Delta G_{-1}^{\ddagger^\circ} = -RT\ ln\left(\frac{k_{-1} h}{k_B T}\right) \quad \text{Eq. 13}$$

$$\Delta G_2^{\ddagger^\circ} = -RT\ ln\left(\frac{k_2 h}{k_B T}\right) \quad \text{Eq. 14}$$

$$\Delta G_{-2}^{\ddagger^\circ} = -RT\ ln\left(\frac{k_{-2} h}{k_B T}\right) \quad \text{Eq. 15}$$

where $\Delta G^{\ddagger^\circ}$ is the variation of the standard activation Gibbs free energy of the specific step (kJ mol^{-1}), R is the gas constant, T is temperature (K), and h and k_B are the Planck and Boltzmann constants, respectively. In addition, Gibbs free energies for the global process ΔG_A° (kJ mol^{-1}) and for the transitions states steps ΔG_{TS1}° and ΔG_{TS2}° (kJ mol^{-1}) were obtained as follow (Menezes et al., 2012; Nazari et al., 2006):

$$\Delta G_A^\circ = -\Delta G_{AC}^\circ = RT\ ln\ K_{AC} \quad \text{Eq. 16}$$

$$\Delta G_{TS1}^\circ = \Delta G_A^\circ + \Delta G_1^{\ddagger\circ} \quad \text{Eq. 17}$$

$$\Delta G_{TS2}^\circ = -\Delta G_{-2}^{\ddagger\circ} \quad \text{Eq. 18}$$

where K_{AC} is the global equilibrium constant [(k_1/k_{-1})(k_2/k_{-2})].

Lastly, by plotting ln(K) *vs* 1/T (Fig. S5b) we have a straight line that provides the standard enthalpy ($\Delta H°$) and entropy changes ($\Delta S°$) from its slope and intercept, respectively (Liu, 2009).

3 RESULTS AND DISCUSSION

3.1 P sorption and temperature

The rise in temperature increases P adsorption on goethite (13.34, 18.11 and 24.23 µmol g^{-1} P at 278, 298 and 323 K, respectively) (Figure 3a-c), but decreases the proportion of P desorbed (48, 28 and 23 % of the adsorbed P at 278, 298 and 323 K, respectively) (Figure 3d). This corroborates to the well-known chemisorption character of P sorption on goethite (Bache, 1964; Belchior et al., 2015; Holtan et al., 1988) but also gives evidence that endothermic steps like goethite precipitation have a relevant participation in the P sorption mechanism (Lyngsie et al., 2014). Such precipitate, favored by higher temperatures, would increase the overall disappearing of P from the solution (accounted within the sorption process), but would also be more stable under the same higher temperatures, releasing (desorbing) less P. Previous studies on P sorption mechanism using isothermal titration calorimetric (ITC) reported an exothermic pattern of the initial stage of the reaction (surface complex formation) that is replaced over time by an endothermic pattern linked to the P-Al and P-Fe precipitation (Lyngsie et al., 2014; Penn et al., 2014; Penn and Warren, 2009; Penn and Zhang, 2010). The kinetic profile of P sorption does not provide details about the reactions taking place in the P sorption mechanism (Figure 3d), but it provides insights into the exo-endothermic nature as well as the amount of mass transferred over time by these reactions (Nazari et al., 2006).

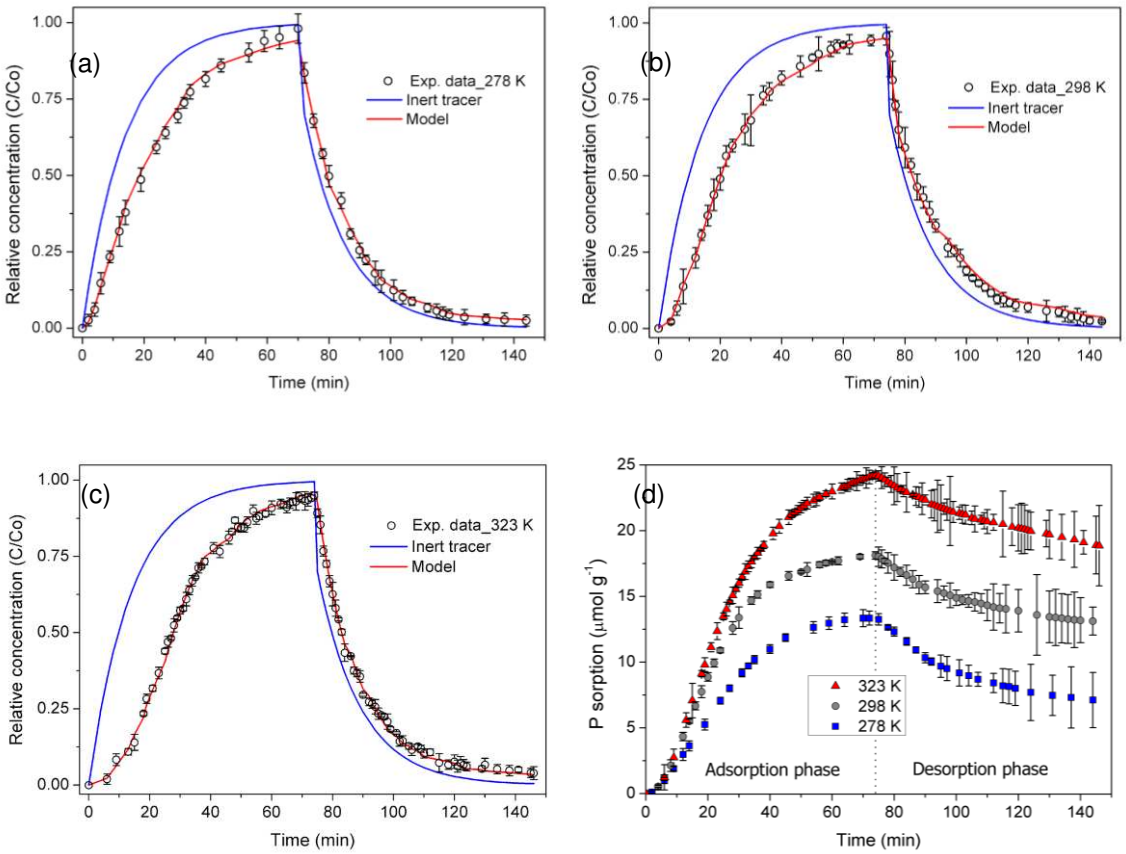

Figure 3. Adsorption/desorption experimental data (open circles – A species), adsorption/desorption simulated curve (red line – A species modeled for mechanism 1), and inert tracer curve (blue line, without sorbent) at 278 K (a), 298 K (b) and 323 K (c). The gap between the experimental data (open circles – A species) and the inert tracer curve (blue line) provides the amount of P adsorbed/desorbed onto goethite at 278, 298 and 323 K (d).

3.2 Kinetic modeling

Investigating the adsorption/desorption process in a single test is an advantage of stirred-flow systems, allowing for a more robust assessment of the sorption mechanisms (Sun and Selim, 2019). From the two initial mechanisms proposed, which represent mechanisms of phosphate sorption onto minerals based on sorption and speciation studies, the kinetic modeling shows that mechanism 1 was a good fit for all temperatures (278, 298, and 323K), with modeled errors lower than the experimental ones (Table 1). Sun et al. (2019) reported that a two-step multi-reactional model like mechanism 1 also simulated well the molybdate sorption onto soils, an oxyanion like phosphate. On the other hand, mechanism 2 resulted in higher modeled error than the experimental error for temperatures of 278 and 298 K, showing a poorer fit. However, there is a trend in decreasing the modeled error for mechanism 2 with the increase in temperature, going from 17.75 % (278 K) to 11.32 % (298 K) and reaching 4.97 % (323 K) (Table 1), an error even lower than that

for mechanism 1. Even though mechanism 1 has shown the best fit in the overall experiment, this temperature effect on mechanism 2 shows that the whole sorption phenomena of P sorbing onto goethite at the experimental conditions used here starts to show a pattern of having two separate and non-dependent steps for the P in the solution, going straight to either B or C species.

Table 1. Kinetic constants of the proposed mechanisms 1 and 2 in different temperatures.

Parameters	**Temperature**		
	278 K	298 K	323 K
Mechanism 1			
k_1 (s^{-1})	$2.61 \times 10^{-3} \pm 1.3 \times 10^{-4}$	$1.88 \times 10^{-3} \pm 2.0 \times 10^{-4}$	$1.34 \times 10^{-3} \pm 1.1 \times 10^{-4}$
k_{-1} (s^{-1})	$3.03 \times 10^{-6} \pm 1.2 \times 10^{-7}$	$3.48 \times 10^{-6} \pm 3.5 \times 10^{-7}$	$4.27 \times 10^{-6} \pm 3.7 \times 10^{-7}$
k_2 (s^{-1})	$4.72 \times 10^{-4} \pm 2.4 \times 10^{-5}$	$5.16 \times 10^{-4} \pm 9.1 \times 10^{-5}$	$5.71 \times 10^{-4} \pm 2.4 \times 10^{-5}$
k_{-2} (s^{-1})	$2.21 \times 10^{-5} \pm 2.2 \times 10^{-6}$	$1.65 \times 10^{-5} \pm 1.2 \times 10^{-7}$	$1.54 \times 10^{-5} \pm 4.1 \times 10^{-7}$
*Error (%)	6.73	8.98	5.94
#Exp. Error (%)	7.54	11.08	6.81
Mechanism 2			
k_1 (s^{-1})	$2.19 \times 10^{-3} \pm 3.2 \times 10^{-5}$	$1.15 \times 10^{-3} \pm 3.6 \times 10^{-4}$	$1.23 \times 10^{-3} \pm 3.0 \times 10^{-5}$
k_{-1} (s^{-1})	$2.58 \times 10^{-5} \pm 3.3 \times 10^{-6}$	$3.26 \times 10^{-5} \pm 3.2 \times 10^{-5}$	$1.38 \times 10^{-5} \pm 4.1 \times 10^{-6}$
k_2 (s^{-1})	$4.04 \times 10^{-4} \pm 4.3 \times 10^{-5}$	$5.18 \times 10^{-4} \pm 1.8 \times 10^{-4}$	$1.07 \times 10^{-3} \pm 2.3 \times 10^{-6}$
k_{-2} (s^{-1})	$9.93 \times 10^{-5} \pm 1.1 \times 10^{-4}$	$6.67 \times 10^{-6} \pm 3.5 \times 10^{-6}$	$2.75 \times 10^{-4} \pm 4.5 \times 10^{-7}$
*Error (%)	17.75	11.32	4.97
#Exp. Error (%)	7.54	11.08	6.81

*Mean absolute percentage error between calculated and experimental vectors with n data $\left(\frac{1}{n}\sum_{j=1}^{n}\frac{|Pexp_j - Pcal_j|}{Pexp_j} \times 100\right)$; #Experimental error based on standard deviation of two repetitions $(\frac{1}{n}\sum_{j=1}^{n}\frac{standard\ deviation_j}{mean_j} \times 100)$.

Mechanism 1 indicates that there is a dependency between B and C species and that the kinetic constants of both B (k_1) and C (k_2) species formation (steps 1 and 2, respectively) are faster than its backward constants (k_{-1} and k_{-2}) (Table 1). As the forward step 2 constant is lower than step 1 ($k_2 < k_1$) and its backward constant is greater ($k_{-2} > k_{-1}$), C species is less stable than B species. This behavior can be verified by modeling concentrations of B and C species from the obtained kinetic constants (Table 1), as presented in Figure 4. On the other hand, it is interesting to notice that for mechanism 2 at the highest temperature (323 K) k_{-2} is still higher than k_{-1}, but k_1 and k_2 present the same order of magnitude, showing that C species formation is favored at higher temperatures.

Using diffusive gradient thin-films (DGT) technique, Menezes-Blackburn et al. (2019) obtained an average rate constant of 8.62×10^{-4} s^{-1} for the desorption of P from 10 soils, a value 50 fold greater than the one obtained here ($k_{-2} = 1.65 \times 10^{-5}$ s^{-1}). On the other hand, Smolders et al. (2021), using a different desorption method and different soils obtained P desorption kinetic rates of 6-16 fold lower than the ones obtained here. These contrasting results are due to methodological differences and to the fact that here we are working with a single pure mineral, while these studies are studying soils with contrasting mineralogy and solution ionic concentration. However, having our desorption rate within the range of different studies working with contrasting soils is important to show that we are working within the range of kinetic constants really controlling the behavior of P in the environment.

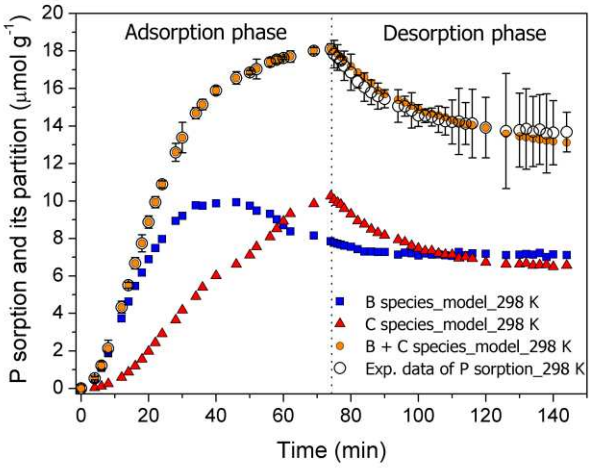

Figure 4. Experimental and modeled data of P sorption and its partition into B and C species overtime at 298 K following mechanism 1. The sum of these species (B and C) represents the experimental data of adsorbed/desorbed P at 298 K.

The formation of B species in the adsorption phase controls the removal of P from the solution in the beginning of the experiment when P concentration in the solution is still low (Figure 4). With the continuous increase on P concentration in the reactor throughout time, C species starts to form, ending up being the most important species controlling the removal of P from the solution in these experimental conditions. Considering the total amount of P adsorbed at 298 K (18.11 µmol g^{-1}), C species corresponds to 57 % of the adsorbed P (10.32 µmol g^{-1}) while B species represents 43 % (7.79 µmol g^{-1}) (Figure 4). In the desorption phase, as the C species present a lower equilibrium constant than B species ($k_2/k_{-2} < k_1/k_{-1}$), C is desorbing more P (74 % - 3.75 µmol g^{-1}) than B species (26 % - 1.32 µmol g^{-1}) (Figure 4).

3.3 P sorption mechanism

Mechanism 1 showed the best fit to the experimental data for the temperatures of 278 and 298 K, with an error lower than that of the experimental data. This mechanism assumes that the P in the bulk solution (A species) adsorbs on sites in the solid-liquid interface (B species), and then forms a third C species, which should be something like a precipitate (Figure 5).

In agreement with this kinetic mechanism of P sorption, Wang et al. (2019, 2017) using a wide range of soil chemical conditions and a set of spectroscopic techniques (nuclear magnetic resonance, infrared, and synchrotron-based X-ray diffraction and absorption) reported that the P in the bulk solution is adsorbed onto the surface of Al or Fe hydroxides as bidentate surface complexes. This has also been shown elsewhere (Abdala et al., 2015a), particularly at low P concentrations (slow P loading) as the one used in this work (100 µmol L^{-1} P). Then, this surface complex behaves as a ternary complex with newly formed negative charges that binds the Al and/or Fe released from the solid-liquid interface, leading to the precipitation of Al and/or Fe phosphates analogues on the surface (surface precipitation) (Figure 5). Changes in the surface electric potential are consonant with the described mechanism, which becomes more negative after P adsorption (Bowden et al., 1980; Li and Stanforth, 2000), returning over time to the initial condition due to cations (e.g., Fe from goethite) covering the new surface (Hu et al., 2020; Ler and Stanforth, 2003).

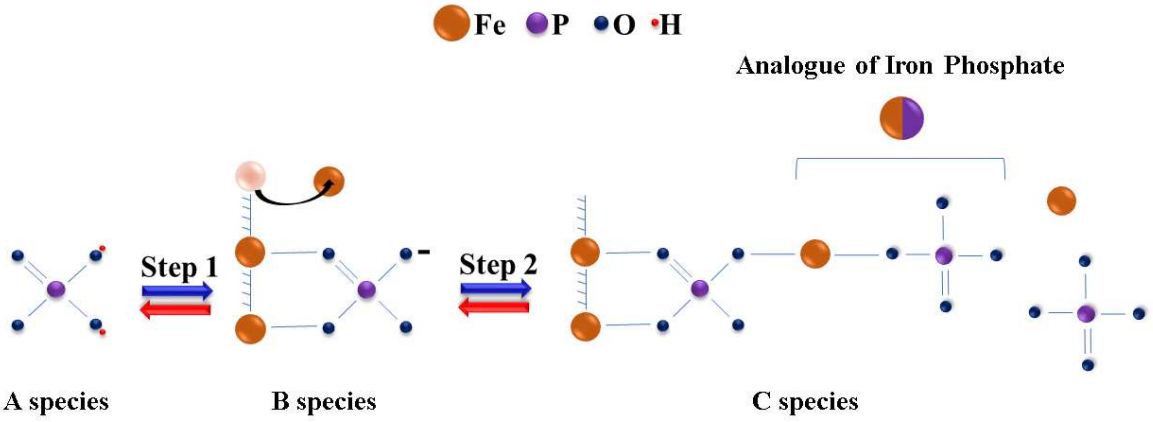

Figure 5. Schematic P sorption mechanism onto goethite surface. Adapted from Ler and Stanforth (2003) , Wang et al. (2019, 2017) and Wang et al. (2018).

Regarding the adsorption of P on goethite, it is already known that it leads to a partial dissolution of the surface of the goethite and to an increase of Fe concentration in the solution (Ler and Stanforth, 2003; Li and Stanforth, 2000). The presence of Fe and/or Al in solution released by the mineral surface due to P adsorption favors the complexation and/or surface and bulk solution

precipitation of Fe and/or Al-P, particularly in batch (closed) adsorption systems with high P initial concentration (15 mmol L^{-1}) and longer time (24 h or more) (Hu et al., 2020; Wang et al., 2018, 2019, 2017). However, the extent of this complexation/precipitation in stirred-flow (open) systems will be lower due to the lower P concentrations applied and the removal of the cations being released by the mineral surface during the adsorption process by the continuous flow.

Here we also confirmed the partial dissolution occurring on the goethite surface due to the adsorption of P (Figure 6). In the beginning of the purge phase of the experiment (0-36 min), when only the background solution (pH 5 and 10 µmol L^{-1} KCl) is passed through the system, we have the concentration of Fe in equilibrium with goethite, kept by its dissolution rate. After removing the Fe in equilibrium with the goethite, the 1 mL min^{-1} flow is enough to keep the Fe concentration in the chamber virtually zero until the adsorption starts. After the P solution starts to flow into the chamber at 36 min we have another peak of Fe release (Figure 6), coming from the dissolution of goethite forced by the P adsorption onto goethite surface. For the first 20 min of the adsorption phase (36-56 min – Fig. 6) we have Fe being removed from the system. From the shape of the curve of the Fe release, it seems that there are 2-3 major events releasing Fe from the goethite during its loading with P and that the dissolution of the goethite starts right after the first injection.

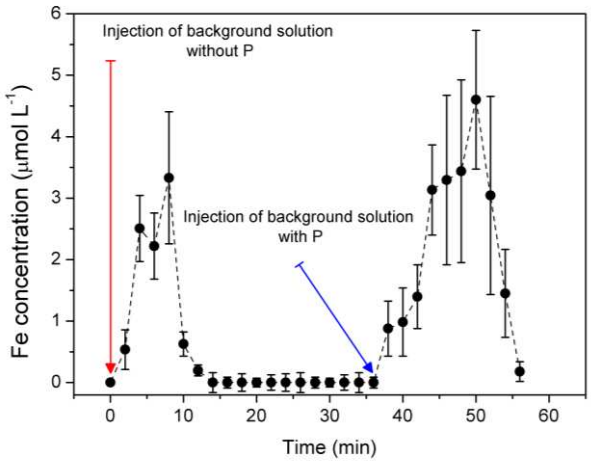

Figure 6. Fe concentration in the effluent of the stirred-flow system during the purge stage (0-36 min) and the P loading phase on goethite (36-56 min) (ICP-OES, Spectro Blue, Spectro Analytical Instruments, Germany). The first peak (purge stage) correspond to Fe concentration maintained by the goethite in equilibrium with the background solution and the second peak (adsorption phase) corresponds to Fe released during the P loading onto the goethite surface. Experimental conditions: 298 K, pH 5, 10 µmol L^{-1} KCl, 5 g L^{-1} goethite, flow rate of 1 mL min^{-1} and 100 µmol L^{-1} P.

Such information has important environmental implications, as it shows that even at a low P concentration as the one used here (100 µmol L^{-1}) the adsorption is able to destabilize the goethite

and release Fe into the solution, setting the conditions for an additional process to happen, precipitation. Even though we are working with a continuous (open) flow system, where the released Fe ions are removed from the system at some point (Figure 6) and P concentration is kept relatively low, stability diagrams show that precipitation still takes place. The log(Fe)-pH stability diagram for Fe species at the same P concentration as used here (Figure 7a) shows that strengite (a partially soluble hydrated Fe-P mineral) is the predominant phase in oxidized systems (e.g., Oxisols) at a wide range of acidic pH (<5.1), even at low iron activities in the solution. The log(P)-pH stability diagram for Fe species at an Fe concentration of 1 µmol L^{-1} (Figure 7b) confirms that even at such low Fe concentration we still have the stability of strengite in our experimental conditions. Lastly, the log(Fe)-log(P) stability diagram at pH= 5 (Figure 7c) confirms that the adsorption experiment happened into the strengite stability field, favoring its precipitation even at low Fe concentrations.

This phenomenon should be greater in closed (batch) sorption systems due to the high concentrations of P used to reach maximum adsorption capacity and to the fact that the released Fe stays in the solution. The same way, as the process of P fertilization creates small regions of unusual high P concentration in the soil around the fertilizer granules or where the liquid/powder fertilizer is applied, P precipitation following the initial adsorption on Fe oxides should be playing a major role in controlling the fate and behavior of P in the environment.

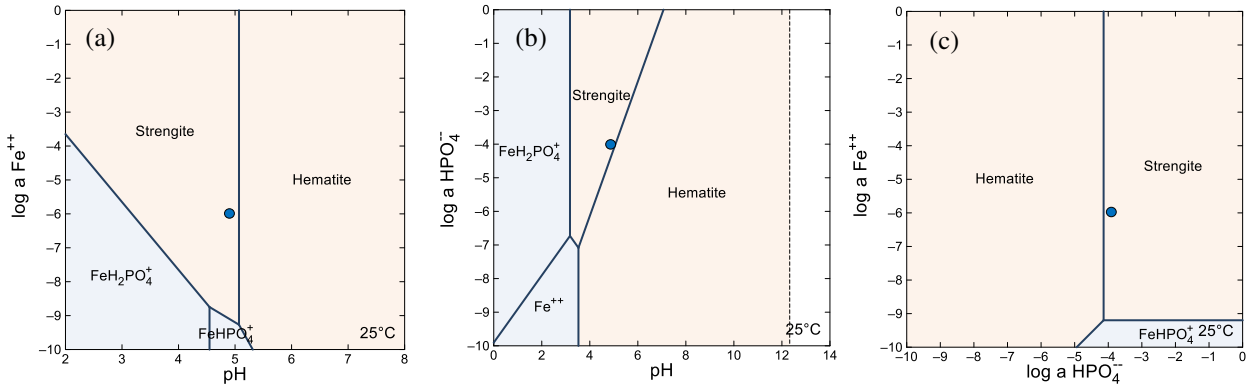

Figure 7. (a)The log(Fe)-pH stability diagram for (HPO_4^{2-}) = 10^{-4} mol L^{-1} (100 µmol L^{-1}). (b)The log(P)-pH stability diagram for (Fe^{2+}) = 10^{-6} mol L^{-1} (1 µmol L^{-1}). (c)The log(Fe)-log(P) stability diagram for pH= 5. All diagrams were built considering P = 1.013bars, Eh= +0.5V, and 298.15 K (25°C), based on GWB software database (Bethke, 2008). Blue dot represents our experimental conditions on the strengite phase.

3.4. P sorption mechanism on phosphate loaded goethite

On a second experiment we proceeded with the same sorption experiment already explained above using the same conditions (pH 5, KCl 10 mmol L^{-1} and 100 µmol L^{-1} of P). Once the goethite

was fully loaded with P (P concentration of the solution leaving the reactor is the same as the one entering it), we stopped the process, collected the goethite from the reactor, and let it rest for 20 days for the P reactions with goethite to age. After that, this pre-loaded goethite was placed again within the reactor and went through the same adsorption experiment again, with the same conditions. Even though it has been fully loaded before, goethite surface has renewed part of its P adsorption capacity and was able to adsorb more 6.24 μmol g^{-1} P, from which 54 % was desorbed afterwards (Figure 8b). As the desorption had not stabilized yet, if the experiment was longer the total amount of P desorbed would be even higher. The lower adsorption capacity compared to the initial pristine goethite is associated with changes in the zeta potential of the new surface resulting in more negative charges and lower availability of adsorption sites for P (Barrow et al., 2018; Ler and Stanforth, 2003; Li and Stanforth, 2000). On the other hand, a greater desorption capacity indicates weaker interactions between P and the new surface, *i.e.,* faster reactions with low $\Delta G^{\ddagger\circ}$, which reflects positively on the P availability to plants. These results explain in part the better agronomic effectiveness of subsequent P fertilizations in highly weathered soils (Barrow, 2015; Barrow et al., 2018; Roy et al., 2017).

The kinetic profile of the first experiment of P sorption (Figure 3d) is different from the P sorption on the already loaded goethite (Figure 8b), indicating that the sorption mechanism has changed, which was expected as the goethite surface is not the same after the first P adsorption. This change in the mechanism was also reaffirmed by the failure of the simulation of the P sorption data (second sorption experiment on phosphate-preloaded goethite) with the kinetic constants obtained from the first P sorption experiment (mechanism 1 at 298 K, Table 1). The simulation resulted in errors of 37.0 and 31.3 % for the mechanisms 1 and 2, respectively, which is high compared with the experimental error (11.7 %). These kinetic constants were then optimized by HANN method and resulted in modeled concentrations that are closer to the experimental data (Figure 8a). However, the modeled errors were still higher than the experimental error (11.7 %), *i.e.,* mechanism 1 and 2 were unable to accurately simulate the sorption of the newly P applied.

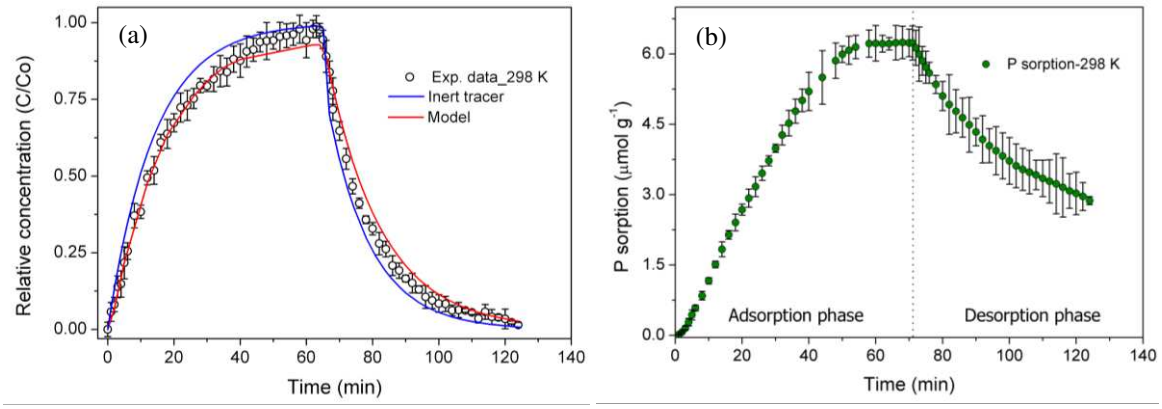

Figure 8. P sorption capacity by P pre-loaded goethite at 298 K. Breakthrough curve of tracer (exp. data - A species), inert tracer and simulated data for mechanism 1 (a). The gap between tracer (exp. data) and inert tracer provides the amount of P sorption over time (b).

Before aging for 20 days, the goethite has been loaded with P to its maximum capacity in equilibrium with the 100 μmol L^{-1} P solution. In principle, there was no more room for additional P adsorption, as the concentration of P leaving the reactor was the same as the one entering it. The same way, there should be no more Fe being released due to the P adsorption onto goethite to bind to the recently adsorbed P, as there was no more Fe being removed from the system after 20 min of the first P injection (Figure 6). However, this new adsorption on the pre-loaded goethite surface (Figure 8b) reached 1/3 of the initial adsorption (Figure 4), which is a relatively high amount for a supposedly fully loaded surface in equilibrium with the used concentration (100 μmol L^{-1} P). Thus, the P adsorption on the pre-loaded goethite after 20 days of aging is the consequence of the renewal of the adsorptive surface, which should be due to a rearrangement of the previously adsorbed P on the surface, opening space for new adsorption, or due to the coverage of the previously adsorbed P by the Fe being released from the dissolution of the goethite.

Even though the new P adsorption on pre-loaded goethite has been relatively high, the desorption has been higher than that for the P adsorbed on pure goethite as well, reaching 50 % in the evaluated time without even stabilizing, indicating that more P would be desorbed if the experiment should be continued (Figure 8). Instead of having the sorbed P and precipitated P as B and C species, respectively, which showed modeled errors higher than the experimental ones, here we would expect to have P more loosely tight to the goethite, probably as outer sphere complexe, for example. This is something important to be understood in our future work, as it represents an important practice in agricultural systems that is the subsequent application of P in the same area, representing a significant fraction of the legacy P (Elser and Bennett, 2011; Smil, 2000).

3.5 Thermodynamic parameters

The kinetic constants provide the energetic mapping of the mechanisms (Borges et al., 2012; Limousin et al., 2007; Liu, 2009; Menezes et al., 2012; Nazari et al., 2006). Estimation of standard activation Gibbs free energy changes ($\Delta G^{\ddagger\circ}$) and standard Gibbs free energy changes (ΔG°) are illustrated in Figure 9a. In step 1, to form the activated complex are necessary 88.59 ±0.31 kJ mol^{-1} ($\Delta G^{\ddagger\circ}$). That amount of energy is needed to overcome the energy barrier related to the activated complex corresponding to the reaction that removes P from the bulk solution (A species) to form the P surface complex (B species); the reverse pathway (B to A species) requires a greater activation energy (104.18 ±0.24 kJ mol^{-1}). In step 2, converting B to C requires 91.79 ±0.04 kJ mol^{-1}, while the reverse pathway (C to B species) needs 100.16 ±0.19 kJ mol^{-1}. Accordingly, Barrow (2020) communicated similar values (60-99 kJ mol^{-1}) of activation energy (an analogue of $\Delta G^{\ddagger\circ}$) for the step 2 (slowest reaction of the P sorption mechanism), but the author related the step 2 to a solid-state diffusion reaction. On the other hand, Torrent (1991) using Barrow's methodology reported values of activation energy between 38-60 kJ mol^{-1} and pointed out that solid-state diffusion reaction is unlikely because the activation energy of this reaction varies greatly for similar samples under the same experimental conditions.

The formation of P surface complexes onto goethite is a spontaneous process for both B and C species (ΔG° = -15.53 ±0.19 kJ mol^{-1} and -8.34 ±0.10 kJ mol^{-1}, respectively) (Figure 9a and 9b). The formation of the B species is the most energetic and its reverse pathway (B to A species) is energetically less favorable compared to the formation of C species, as confirmed by the energetics of the transition-state of step 2 (ΔG°_{TS2} = 100.16 ±0.19 kJ mol^{-1}) and step 1 (ΔG°_{TS1} = 112.69 ±0.21 kJ mol^{-1}) (Figure 9a), pushing the reaction towards the formation of C species.

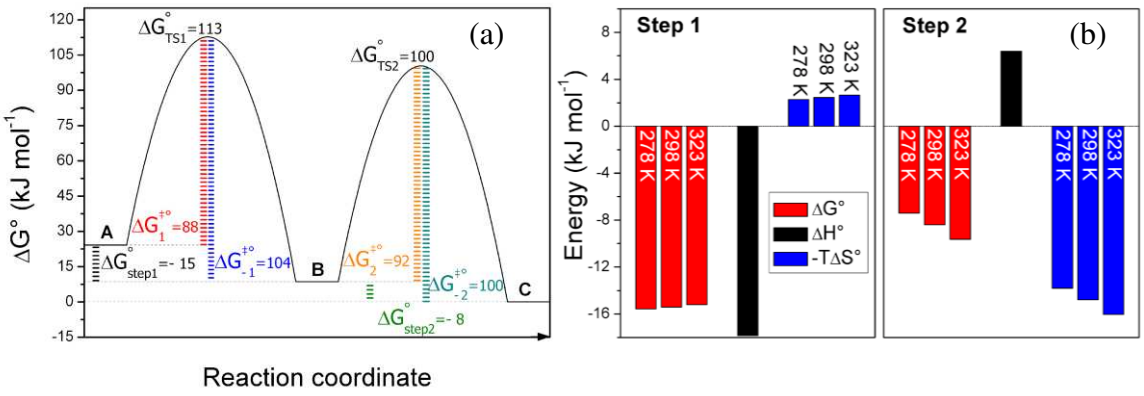

Figure 9. (a) Stepwise standard activation Gibbs free energy changes ($\Delta G^{\ddagger\circ}$) and standard Gibbs free energy changes (ΔG°) for the species involved in mechanism 1 (A ⇌ B⇌ C) of P sorption by

goethite at 298 K. (b) Enthalpic and entropic components (278, 298 and 323 K) of the steps 1 and 2. Experimental conditions: pH 5, 10 mmol L^{-1} KCl and 100 µmol L^{-1} P.

Although both steps were spontaneous at experimental temperatures, the thermodynamic parameters that drive these reactions are different (Figure 9b). Step 1 refers to an enthalpy-driven process ($\Delta H° < T\Delta S°$) with $\Delta H°$ = -16.93 ±1.6 kJ mol^{-1} and $\Delta S°$ = -0.01 ±0.005 kJ K^{-1} mol^{-1}, while step 2 is an entropy-driven process ($\Delta H° > T\Delta S°$) with $\Delta H°$ = 9.04 ±3.4 kJ mol^{-1} and $\Delta S°$ = 0.06±0.02 kJ K^{-1} mol^{-1} (Figure 9b). Therefore, considering the participation of these processes throughout time (Figure 4), an exothermic reaction is controlling the initial phase, which is replaced by an endothermic one in the second phase. These results are in line with those reported by isothermal titration calorimetry-based investigations on soil and soil minerals (Lyngsie et al., 2014; Penn et al., 2014; Penn and Warren, 2009; Penn and Zhang, 2010).

The thermodynamics parameters are useful to better understand the sorption mechanism. In step 1, the low and negative variation of entropy indicates that the system has become slightly more ordered, including the solid-liquid interface (Chen et al., 2017). Although the desolvation of the goethite surface and phosphate ions during the adsorption process contribute to increase the entropy of the system, the formation of the P surface complex reduces the degree of translational freedom of the phosphate ions. Given the net negative $\Delta S°$ of step 1 (Figure 9) the latter effect is dominant and defines the entropic contribution. Besides that, we can also see that there is not much influence of temperature on the thermodynamics of step 1.

Regarding enthalpy changes in step 1, the key processes contributing to the negative enthalpy are the intermolecular interactions between P and hydroxyl groups on goethite surface and the desolvation of water molecules from the goethite surface and from phosphate ions during the adsorption process (Christiano et al., 2015). Part of the energy dissipated to the surroundings is absorbed by the goethite crystalline structure, inducing the goethite dissolution (Cornell et al., 1974; Ler and Stanforth, 2003; Li and Stanforth, 2000; Schwertmann, 1984; Wang et al., 2018), with the goethite dissolution also contributing to the exothermic pattern (Penn and Warren, 2009).

As step 2 is an endothermic reaction ($\Delta H° > 0$) (Figure 9b), the energy released in step 1 feeds it (cascading effects). This energy consumption ($\Delta H° > 0$) should be associated with the P-Fe precipitation at the surface or bulk solution (Penn and Zhang, 2010). Even though precipitations are expected to lead to a net ordering effect to the precipitated ions, the precipitation of ions like Fe^{2+} and $H_2PO_4^-$, also called “electronic structure makers”, give a net disordering effect to the system due to the release of water molecules kept in there hydration spheres. It is also clear that there is a higher influence of temperature on step 2 than 1, with the increase in temperature increasing $\Delta S°$,

and this is in accordance the stability of strengite as well which increases with temperature (Zhang et al., 2017).

3.6 Implications on agricultural environments and fertilizer technology

The kinetic study developed here is related to the sorption of P by goethite in open system, bringing additional information regarding the process of P sorption on goethite to help us understanding the behavior of P in the highly weathered soils aiming to improve P use efficiency. The results described here are in accordance with other studies carried out with soils and pure minerals in open and closed systems, where P adsorption and desorption have a fast initial step followed by a slow one (Guedes et al., 2016; Saki et al., 2020). Understanding and separating these steps under this kinetic approach allowed us to identify that most of the P released during the desorption phase (74 %) came from the structure produced in step 2 (C species) (Figure 4). The highest desorption rate of step 2 indicates that the C species is an important P source for plant nutrition, improving the P labile pool (Barrow, 2020; Smolders et al., 2021). Thus, at least in the short term evaluated here, our fertilizer technologies and management practices should be more focused in avoiding the production of the B species, which is the one contributing the lowest for the released P.

However, the half-life time ($t^{1/2} = \ln 2 / k_{-2}$) corresponding to P desorption rate of the C species is relatively short (~ 0.5 day). Menezes-Blackburn et al. (2019) investigating 10 soils reported a half-life time of 0.01 day, while Smolders et al. (2021) using the a two-step sequential model (the same used in this study) for soils reported a half-life of 3-8 days for the P labile pool. In a plant trial, Rech et al. (2018) monitored the P concentration in the soil solution for 38 days after P fertilization and observed a remarkable reduction in the P concentration (~ 50 %) within 3-4 days. Thus, given the short half-life of the C species formed, particularly the perennial crops might still suffer from P deficiency if relying only in the C species to provide the needed P in later stages of the crop cycle. Here we found that the C species accounted for 57 % of the sorbed P (Figure 4), which would be aligned with the P precipitation on mineral surface corresponding to 60-75 % of the P sorbed at higher P concentrations (Wang et al., 2019). Making an analogy of C species with surface precipitation, it corresponds to the largest P pool of the sorption mechanism.

The kinetic mechanism indicates that the P is rapidly adsorbed by sites on goethite surface forming B species, but that its reverse pathway (B to A, P in solution) requires a greater activation energy (104 kJ mol^{-1}) compared to the other reactions of the P sorption mechanism (Figure 9a). It means that the adsorption of P onto goethite stabilizes even further the already stable goethite in

highly weathered soils, as already assessed elsewhere by different techniques (Fernández R. et al., 2009). Therefore, it seems obvious that to increase the bioavailability of P in such conditions it is necessary to prevent the formation of the B species by adding a "bait" anion that would occupy the P adsorption sites on the mineral surface, as it has already been shown for organic acids like oxalate, malate, and citrate (Hu et al., 2020; Wang et al., 2015, 2018; Weng et al., 2012). This helps clarifying the mechanisms by which soil organic matter increases P availability and it is one of the most effective practices to increase P availability and use efficiency in tropical soils.

Another way to mitigate the sorption of P, particularly the C species formation, is to reduce the Fe activity in the system, especially at solid-liquid interface (Wang et al., 2018). In this sense, the "bait" anion must have an affinity for the mineral surface, but not promoting the mineral dissolution, and have a high affinity for Fe ions (Christensen et al., 2003; Nowack and Sigg, 1996; Wang et al., 2018; Wen et al., 2021). These "bait" anions, particularly the organic acids, can be incorporated into the fertilizer matrix (Borges et al., 2020; Janke et al., 2019; Pogorzelski et al., 2020; Withers et al., 2014) as a fertilizer technology or to be brought into the system by conservation agricultural practices. Having a constant production of organic acids by the decomposition of residues (from the main and cover crops) or root release is also a very important way of improving P use efficiency and to optimize its use.

4 CONCLUSION

The P sorption mechanism presented reactions dependent on each other, *i.e.*, the reactions occurred in sequential steps at 278 and 298 K. Indeed, the first reaction of the mechanism quickly stabilized P on the goethite surface (P surface complex) and acted as a trigger for the second step. The formation of the P surface complex promoted the release of energy to the system, the goethite dissolution and consequently the release of Fe. These conditions and the presence of P at the mineral interface contributed to the occurrence of the second reaction, which resulted in the largest pool of P and showed the highest rate of P desorption, indicating an important contribution to the availability of P to plants.

The tested kinetic models were not able to access the P sorption mechanism by phosphate-pre-loaded goethite, evidencing the need for further investigation. Yet, the phosphate-pre-loaded goethite showed a lower capacity for P adsorption and a greater capacity for desorption facing a new P application, corroborating with previous knowledge that the availability of P in soils increases with subsequent P fertilization. Overall, stirred-flow system and multi-reactional modeling by

HANN were able to provide insights at the molecular level for the P sorption mechanism and their specific steps.

5 GRAPHICAL ABSTRACT

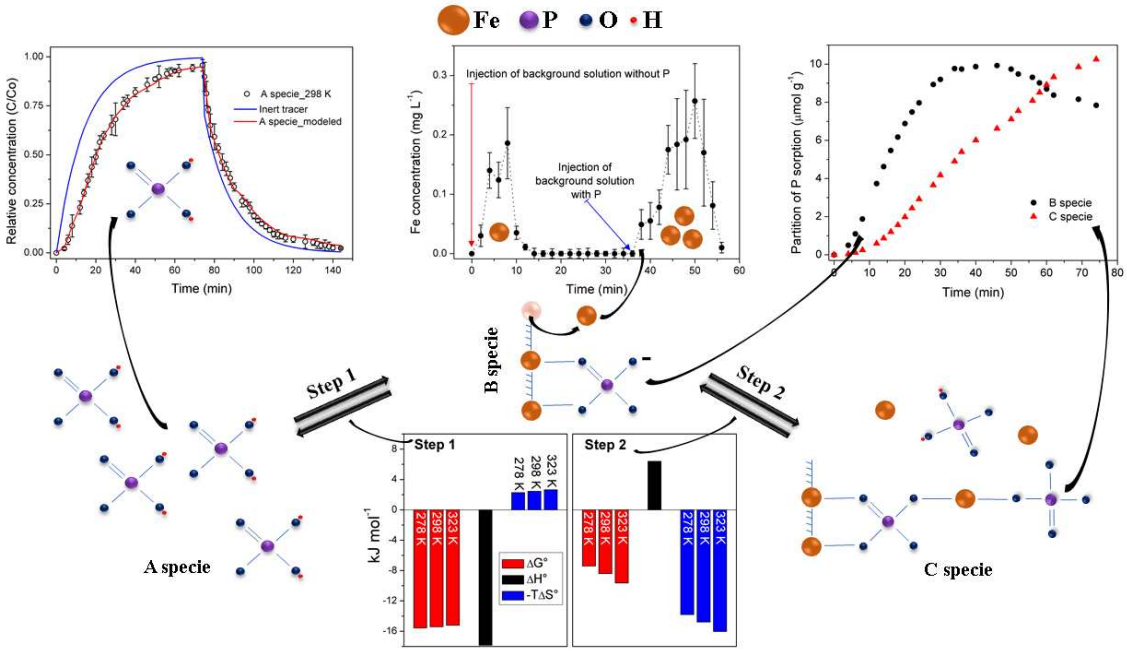

Synopsis. P sorption mechanism on goethite has two key steps that occur in sequence. The step 1 corresponds to an enthalpy-driven process while step 2 is an entropy-driven one. Markedly, the step 1 promotes Fe release and step 2 corresponds to the largest pool of P over time.

6 SUPPLEMENTARY MATERIAL

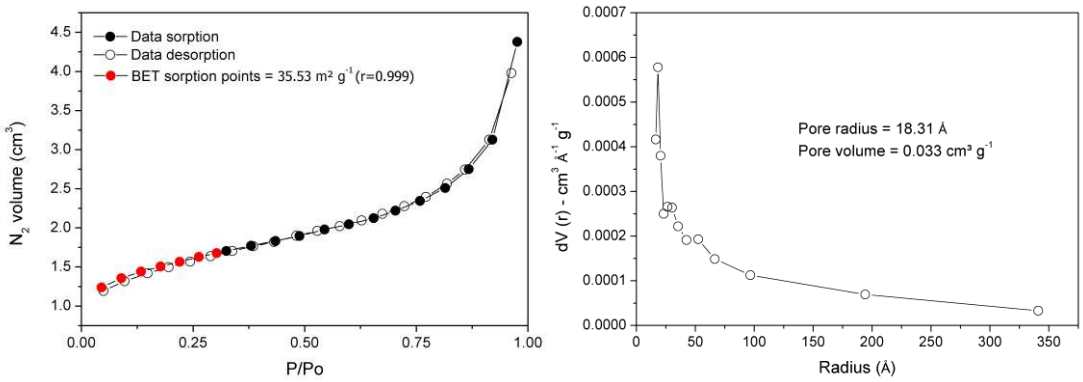

Figure S1. Isotherm of N_2 physisorption (left) on goethite, presenting its specific surface area by BET model on adsorption data. N_2 desorption volume change as function of radius and mineral mass (pore size distribution), presenting the pore radius and pore volume of the goethite by BJH model on desorption data. Overall, goethite presented a low surface area and porosity.

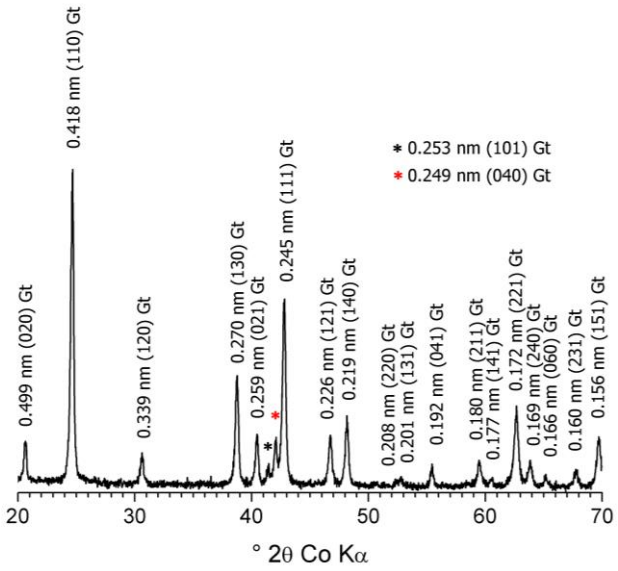

Figure S2. X-ray diffraction of powdered goethite after dialysis. Interplanar distances in nm. The synthetic mineral shows well-defined peaks, indicating good crystallinity.

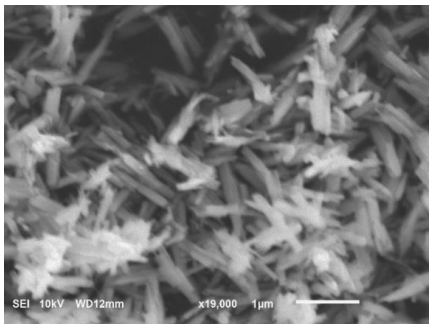

Figure S3. SEM image of goethite acicular crystals after dialysis.

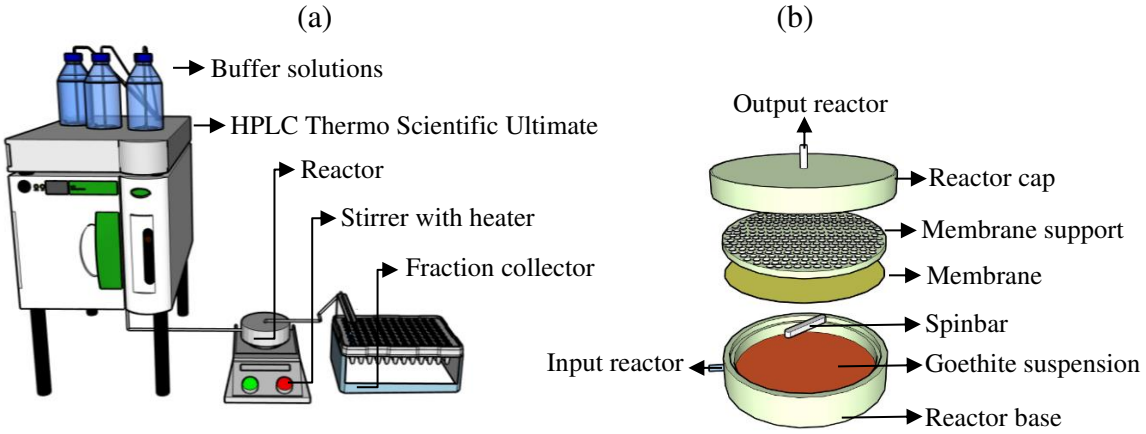

Figure S4. Scheme of the stirred-flow system (a) and reactor parts (b). Reactor has diameter of 4.5 cm and height of 0.9 cm. The cellulose acetate membrane (Sartorius Stedim Biotech) has diameter of 4.5 cm and size porous of 200 nm.

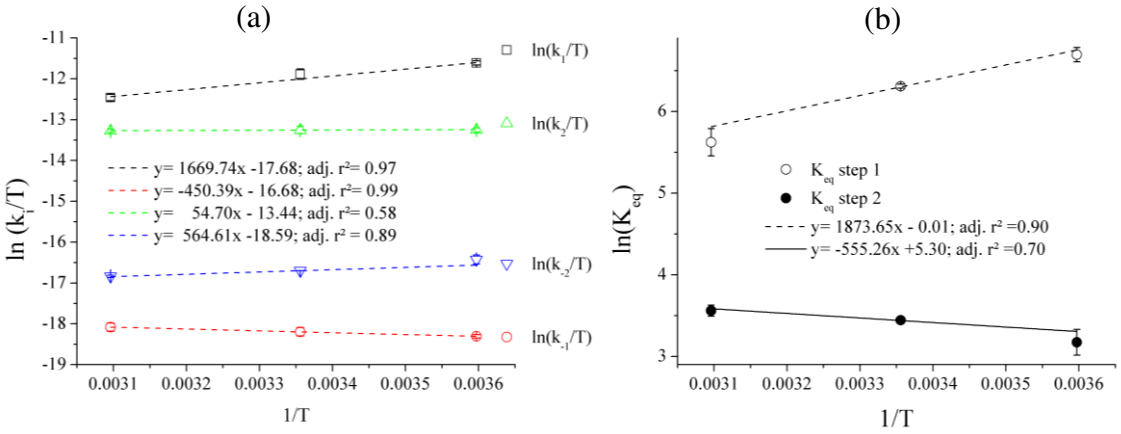

Figure S5. (a) Linearization of Eyring equation provides the standard activation enthalpy change ($\Delta H^{\ddagger\circ}$) and entropy ($\Delta S^{\ddagger\circ}$) from the slope and intercept, respectively (Christiano et al., 2015). (b) The plot ln(K) *vs* 1/T yielded a straight line that provides the standard enthalpy change (ΔH°) and entropy (ΔS°) from the slope and intercept, respectively (Liu, 2009).

7 REFERENCES

Abdala, D.B., Northrup, P.A., Arai, Y., Sparks, D.L., 2015a. Surface loading effects on orthophosphate surface complexation at the goethite/water interface as examined by extended X-ray Absorption Fine Structure (EXAFS) spectroscopy. J. Colloid Interface Sci. 437, 297–303. https://doi.org/10.1016/j.jcis.2014.09.057

Abdala, D.B., Northrup, P.A., Vicentin, F.C., Sparks, D.L., 2015b. Residence time and pH effects on the bonding configuration of orthophosphate surface complexes at the goethite/water interface as examined by Extended X-ray Absorption Fine Structure (EXAFS) spectroscopy. J. Colloid Interface Sci. 442, 15–21. https://doi.org/10.1016/j.jcis.2014.11.048

Arai, Y., Sparks, D.L., 2001. ATR-FTIR spectroscopic investigation on phosphate adsorption mechanisms at the ferrihydrite-water interface. J. Colloid Interface Sci. 241, 317–326. https://doi.org/10.1006/jcis.2001.7773

Bache, B.W., 1964. Aluminium and Iron Phosphate Studies Relating To Soils: Ii. Reactions Between Phosphate and Hydrous Oxides. J. Soil Sci. 15, 110–116. https://doi.org/10.1111/j.1365-2389.1964.tb00250.x

Bar-Tal, A., Feigenbaum, S., Sparks, D.L., Pesek, J.D., 1990. Analyses of Adsorption Kinetics Using a Stirred-Flow Chamber: I. Theory and Critical Tests. Soil Sci. Soc. Am. J. 54, 1273–1278. https://doi.org/10.2136/sssaj1990.03615995005400050012x

Barrett, E.P., Joyner, L.G., Halenda, P.P., 1951. The determination of pore volume and area distributions in porous substances. I. computations from nitrogen isotherms. J. Am. Chem. Soc. 73, 373–380. https://doi.org/10.1021/ja01145a126

Barrow, N.J., 2020. Comparing two theories about the nature of soil phosphate. Eur. J. Soil Sci. https://doi.org/10.1111/ejss.13027

Barrow, N.J., 2015. Soil phosphate chemistry and the P-sparing effect of previous phosphate applications. Plant Soil 397, 401–409. https://doi.org/10.1007/s11104-015-2514-5

Barrow, N.J., 1983. A mechanistic model for describing the sorption and desorption of phosphate by soil. J. Soil Sci. 34, 733–750. https://doi.org/10.1111/ejss.12198

Barrow, N.J., Barman, P., Debnath, A., 2018. Three Residual Benefits of Applying Phosphate

Fertilizer. Soil Sci. Soc. Am. J. 82, 1168. https://doi.org/10.2136/sssaj2018.03.0115

Belchior, D., Andrew, P., Arai, Y., Lewis, D., 2015. Journal of Colloid and Interface Science Surface loading effects on orthophosphate surface complexation at the goethite / water interface as examined by extended X-ray Absorption Fine Structure (EXAFS) spectroscopy. J. Colloid Interface Sci. 437, 297–303. https://doi.org/10.1016/j.jcis.2014.09.057

Borges, B.M.M.N., Strauss, M., Camelo, P.A., Sohi, S.P., Franco, H.C.J., 2020. Re-use of sugarcane residue as a novel biochar fertiliser - Increased phosphorus use efficiency and plant yield. J. Clean. Prod. 262, 121406. https://doi.org/10.1016/j.jclepro.2020.121406

Borges, E., Menezes, D.C., 2017. Resolução De Problemas Inversos Em Cinética Química Usando Redes Neuronais Artificiais. J. Eng. Exact Sci. 3, 436–453. https://doi.org/10.18540/jcecvl3iss3pp436-453

Borges, E., Menezes, D.C., Braga, J.P., 2012. An Ill-posed inverse problem in enzymatic kinetics: Jack-Bean urease denaturation by an anionic surfactant. Int. J. Quantum Chem. https://doi.org/10.1002/qua.24163

Bowden, J.W., Nagarajah, S., Barrow, N.J., Posner, A.M., Quirk, J.P., 1980. Describing the adsorption of phosphate, citrate and selenite on a variable-charge mineral surface. Aust. J. Soil Res. https://doi.org/10.1071/SR9800049

Brunauer, S., Emmett, P.H., Teller, E., 1938. Adsorption of Gases in Multimolecular Layers. J. Am. Chem. Soc. 60, 309–319. https://doi.org/citeulike-article-id:4074706\rdoi: 10.1021/ja01269a023

Chen, P., Nishiyama, Y., Wohlert, J., Lu, A., Mazeau, K., Ismail, A.E., 2017. Translational Entropy and Dispersion Energy Jointly Drive the Adsorption of Urea to Cellulose. J. Phys. Chem. B. https://doi.org/10.1021/acs.jpcb.6b11914

Chen, Y.S.R., Butler, J.N., Stumm, W., 1973. Kinetic Study of Phosphate Reaction with Aluminum Oxide and Kaolinite. Environ. Sci. Technol. https://doi.org/10.1021/es60076a007

Christensen, T., Gooden, D.M., Kung, J.E., Toone, E.J., 2003. Additivity and the physical basis of multivalency effects: A thermodynamic investigation of the calcium EDTA interaction. J. Am. Chem. Soc. 125, 7357–7366. https://doi.org/10.1021/ja021240c

Christiano, B., Ferreira, S., Simões, F., Barbosa, A., Frédéric, L., Pereira, R., Freitas, D., Vinícius, L., Gurgel, A., 2015. Application of a new carboxylate-functionalized sugarcane bagasse for adsorptive removal of crystal violet from aqueous solution : Kinetic , equilibrium and thermodynamic studies. Ind. Crop. Prod. 65, 521–534. https://doi.org/10.1016/j.indcrop.2014.10.020

Condron, L.M., Turner, B.L., Cade-Menun, B.J., 2015. Chemistry and Dynamics of Soil Organic Phosphorus. https://doi.org/10.2134/agronmonogr46.c4

Cornell, R.M., Posner, A.M., Quirk, J.P., 1974. Crystal morphology and the dissolution of goethite. J. Inorg. Nucl. Chem. https://doi.org/10.1016/0022-1902(74)80705-0

dos Santos Teixeira, A.F., Henrique Procópio Pelegrino, M., Missina Faria, W., Henrique Godinho Silva, S., Gabriela Marcolino Gonçalves, M., Weimar Acerbi Júnior, F., Rezende Gomide, L., Linares Pádua Júnior, A., de Souza, I.A., Chakraborty, S., Weindorf, D.C., Roberto Guimarães Guilherme, L., Curi, N., 2020. Tropical soil pH and sorption complex prediction via portable X-ray fluorescence spectrometry. Geoderma 361, 114132. https://doi.org/10.1016/j.geoderma.2019.114132

Eick, M.J., Bar-tal, A., Sparks, D.L., Feigenbaum, S., 1990. Analyses of Adsorption Kinetics Using a Stirred-Flow Chamber : II . Potassium-Calcium Exchange on Clay Minerals. Soil Sci. Soc. Am. J. 54, 1278–1282. https://doi.org/10.2136/sssaj1990.03615995005400050013x

Elser, J., Bennett, E., 2011. Phosphorus cycle: A broken biogeochemical cycle. Nature 478, 29–31. https://doi.org/10.1038/478029a

Eriksson, A.K., Hesterberg, D., Klysubun, W., Gustafsson, J.P., 2016. Phosphorus dynamics in Swedish agricultural soils as influenced by fertilization and mineralogical properties: Insights gained from batch experiments and XANES spectroscopy. Sci. Total Environ. https://doi.org/10.1016/j.scitotenv.2016.05.225

Eyeing, H., 1935. The activated complex and the absolute rate of chemical reactions. Chem. Rev. https://doi.org/10.1021/cr60056a006

Fernández-Calviño, D., Pérez-Novo, C., Bermúdez-Couso, A., López-Periago, E., Arias-Estévez, M., 2010. Batch and stirred flow reactor experiments on Zn sorption in acid soils. Cu competition. Geoderma 159, 417–424. https://doi.org/10.1016/j.geoderma.2010.09.007

Fernández R., I.E., Novais, R.F., Nunes, F.N., Ker, J.C., 2009. Reversibility of non-labile phosphorus in soils under microbial and chemical reduction. II - Successive anion exchange resin extraction of phosphorus. Rev. Bras. Cienc. do Solo 32, 2319–2330. https://doi.org/10.1590/s0100-06832008000600011

Fink, Jessé, R., Inda, A.V., Tiecher, T., Barrón, V., 2016. Iron oxides and organic matter on soil phosphorus availability. Cienc. e Agrotecnologia 40, 369–379. https://doi.org/10.1590/1413-70542016404023016

Gérard, F., 2016. Clay minerals, iron/aluminum oxides, and their contribution to phosphate sorption in soils - A myth revisited. Geoderma 262, 213–226. https://doi.org/10.1016/j.geoderma.2015.08.036

Guedes, R.S., Melo, L.C.A., Vergütz, L., Rodríguez-Vila, A., Covelo, E.F., Fernandes, A.R., 2016. Adsorption and desorption kinetics and phosphorus hysteresis in highly weathered soil by stirred flow chamber experiments. Soil Tillage Res. 162, 46–54. https://doi.org/10.1016/j.still.2016.04.018

Gustafsson, J.P., Braun, S., Marius Tuyishime, J.R., Adediran, G.A., Warrinnier, R., Hesterberg, D., 2020. A probabilistic approach to phosphorus speciation of soils using p k-edge xanes spectroscopy with linear combination fitting. Soil Syst. 4, 1–17. https://doi.org/10.3390/soilsystems4020026

Holtan, H., Kamp-Nielsen, L., Stuanes, A.O., 1988. Phosphorus in Soil, Water and Sediment: An Overview, in: Phosphorus in Freshwater Ecosystems. Springer Netherlands, Dordrecht, pp. 19–34. https://doi.org/10.1007/978-94-009-3109-1_3

Hopfield, J.J., 1984. Neurons with graded response have collective computational properties like those of two-state neurons. Proc. Natl. Acad. Sci. U. S. A. https://doi.org/10.1073/pnas.81.10.3088

Hopfield, J.J., Tank, D.W., 1985. “Neural” computation of decisions in optimization problems. Biol. Cybern. https://doi.org/10.1007/BF00339943

Hu, Z., Jaisi, D.P., Yan, Y., Chen, H., Wang, X., Wan, B., Liu, F., Tan, W., Huang, Q., Feng, X., 2020. Adsorption and precipitation of myo-inositol hexakisphosphate onto kaolinite. Eur. J. Soil Sci. https://doi.org/10.1111/ejss.12849

Janke, C.K., Fujinuma, R., Moody, P., Bell, M.J., 2019. Biochemical effects of banding limit the benefits of nitrification inhibition and controlled-release technology in the fertosphere of high N-input systems. Soil Res. 57, 28. https://doi.org/10.1071/SR18211

Kruse, J., Abraham, M., Amelung, W., Baum, C., Bol, R., Kühn, O., Lewandowski, H., Niederberger, J., Oelmann, Y., Rüger, C., Santner, J., Siebers, M., Siebers, N., Spohn, M., Vestergren, J., Vogts, A., Leinweber, P., 2015. Innovative methods in soil phosphorus research: A review. J. Plant Nutr. Soil Sci. 178, 43–88. https://doi.org/10.1002/jpln.201400327

Lemes, N.H.T., Borges, E., Braga, J.P., 2009. Rate constants and absorption coefficients from experimental data: An inversion procedure based on recursive neural networks. Chemom. Intell. Lab. Syst. 96, 84–87. https://doi.org/10.1016/j.chemolab.2009.01.006

Lemes, N.H.T., Borges, E., Sousa, R. V., Braga, J.P., 2008. Potential energy function from differential cross-section data: An inverse quantum scattering theory approach. Int. J. Quantum Chem. 108, 2623–2627. https://doi.org/10.1002/qua.21701

Ler, A., Stanforth, R., 2003. Evidence for surface precipitation of phosphate on goethite. Environ. Sci. Technol. https://doi.org/10.1021/es020773i

Li, L., Stanforth, R., 2000. Distinguishing Adsorption and Surface Precipitation of Phosphate on Goethite (α-FeOOH). J. Colloid Interface Sci. 230, 12–21. https://doi.org/10.1006/jcis.2000.7072

Li, W., Feng, X., Yan, Y., Sparks, D.L., Phillips, B.L., 2013. Solid-state NMR spectroscopic study of phosphate sorption mechanisms on aluminum (hydr)oxides. Environ. Sci. Technol. 47, 8308–8315. https://doi.org/10.1021/es400874s

Limousin, G., 2007. Sorption isotherms : A review on physical bases , modeling and measurement. Appl. Geochemistry 22, 249–275. https://doi.org/10.1016/j.apgeochem.2006.09.010

Limousin, G., Gaudet, J.P., Charlet, L., Szenknect, S., Barthès, V., Krimissa, M., 2007. Sorption isotherms: A review on physical bases, modeling and measurement. Appl. Geochemistry 22, 249–275. https://doi.org/10.1016/j.apgeochem.2006.09.010

Liu, Y., 2009. Is the free energy change of adsorption correctly calculated? J. Chem. Eng. Data 54, 1981–1985. https://doi.org/10.1021/je800661q

Lyngsie, G., Penn, C.J., Hansen, H.C.B., Borggaard, O.K., 2014. Phosphate sorption by three potential filter materials as assessed byisothermal titration calorimetry. J. Environ. Manage. 143, 26–33. https://doi.org/10.1016/j.jenvman.2014.04.010

Mendez, J.C., Van Eynde, E., Hiemstra, T., Comans, R.N.J., 2022. Surface reactivity of the natural metal (hydr)oxides in weathered tropical soils. Geoderma 406, 115517. https://doi.org/10.1016/j.geoderma.2021.115517

Menezes-Blackburn, D., Sun, J., Lehto, N.J., Zhang, H., Stutter, M., Giles, C.D., Darch, T., George, T.S., Shand, C., Lumsdon, D., Blackwell, M., Wearing, C., Cooper, P., Wendler, R., Brown, L., Al-Kasbi, M., Haygarth, P.M., 2019. Simultaneous Quantification of Soil Phosphorus Labile Pool and Desorption Kinetics Using DGTs and 3D-DIFS. Environ. Sci. Technol. 53, 6718–6728. https://doi.org/10.1021/acs.est.9b00320

Menezes, D.C., Borges, E., Torres, M.F., Braga, J.P., 2012. A kinetic study of jack-bean urease denaturation by a new dithiocarbamate bismuth compound. Chem. Phys. Lett. https://doi.org/10.1016/j.cplett.2012.07.078

Naidu, R., Bolan, N.S., Kookana, R.S., Tiller, K.G., 1994. Ionic-strength and pH effects on the sorption of cadmium and the surface charge of soils. Eur. J. Soil Sci. 45, 419–429. https://doi.org/10.1111/j.1365-2389.1994.tb00527.x

Nazari, K., Mahmoudi, A., Esmaeili, N., Sadeghian, L., Moosavi-Movahedi, A.A., Khodafarin, R., 2006. Denaturation of jack-bean urease by sodium n-dodecyl sulphate: A kinetic study below the critical micelle concentration. Colloids Surfaces B Biointerfaces. https://doi.org/10.1016/j.colsurfb.2006.08.007

Nowack, B., Sigg, L., 1996. Adsorption of EDTA and metal-EDTA complexes onto goethite. J. Colloid Interface Sci. 177, 106–121. https://doi.org/10.1006/jcis.1996.0011

Penn, C., Camberato, J., 2019. A Critical Review on Soil Chemical Processes that Control How Soil pH Affects Phosphorus Availability to Plants. Agriculture 9, 120. https://doi.org/10.3390/agriculture9060120

Penn, C., Heeren, D., Fox, G., Kumar, A., 2014. Application of Isothermal Calorimetry to Phosphorus Sorption onto Soils in a Flow-through System. Soil Sci. Soc. Am. J. https://doi.org/10.2136/sssaj2013.06.0239

Penn, C.J., Warren, J.G., 2009. Investigating Phosphorus Sorption onto Kaolinite Using Isothermal Titration Calorimetry. Soil Sci. Soc. Am. J. 73, 560. https://doi.org/10.2136/sssaj2008.0198

Penn, C.J., Zhang, H., 2010. Isothermal Titration Calorimetry as an Indicator of Phosphorus Sorption Behavior. Soil Sci. Soc. Am. J. 74, 502–511. https://doi.org/10.2136/sssaj2009.0199

Pérez-Novo, C., Fernández-Calviño, D., Berm??dez-Couso, A., López-Periago, J.E., Arias-Estévez, M., 2011. Influence of phosphorus on Cu sorption kinetics: Stirred flow chamber experiments. J. Hazard. Mater. 185, 220–226. https://doi.org/10.1016/j.jhazmat.2010.09.021

Pogorzelski, D., Filho, J.F.L., Matias, P.C., Santos, W.O., Vergütz, L., Melo, L.C.A., 2020. Biochar as composite of phosphate fertilizer: Characterization and agronomic effectiveness. Sci. Total Environ. 743. https://doi.org/10.1016/j.scitotenv.2020.140604

Rech, IonáRech, I., Withers, P., Jones, D., Pavinato, P., 2018. Solubility, Diffusion and Crop Uptake of Phosphorus in Three Different Struvites. Sustainability 11, 134. doi:10.3390/su11010134, Withers, P., Jones, D., Pavinato, P., 2018. Solubility, Diffusion and Crop Uptake of Phosphorus in Three Different Struvites. Sustainability 11, 134. https://doi.org/10.3390/su11010134

Roy, E.D., Willig, E., Richards, P.D., Martinelli, L.A., Vazquez, F.F., Pegorini, L., Spera, S.A., Porder, S., 2017. Soil phosphorus sorption capacity after three decades of intensive fertilization in Mato Grosso, Brazil. Agric. Ecosyst. Environ. 249, 206–214. https://doi.org/10.1016/j.agee.2017.08.004

Sahu, A., Banerjee, S., Raju, A.S., Chiou, T.J., Rene Garcia, L., Versaw, W.K., 2020. Spatial profiles of phosphate in roots indicate developmental control of uptake, recycling, and sequestration. Plant Physiol. https://doi.org/10.1104/pp.20.01008

Saki, H., Liu, H., Lennartz, B., 2020. Phosphate sorption onto structured soil. Soil Syst. 4, 1–13. https://doi.org/10.3390/soilsystems4020021

Schwertmann, U., 1984. The influence of aluminium on iron oxides: IX. Dissolution of Al-goethites in 6 M HCl . Clay Miner. https://doi.org/10.1180/claymin.1984.019.1.02

Sebastião, R.C.O., Braga, P.J., Virtuoso, L.S., Borges, E., 2011. Retrieval of kinetic rates in reactions with semi batch liquid phase using ill-posed inverse problem theory. Quim. Nova 34, 213–217. https://doi.org/10.1590/S0100-40422011000200008

Seyfried, M.S., Sparks, D.L., Bar-Tal, A., Feigenbaum, S., 1989. Kinetics of Calcium-Magnesium Exchange on Soil Using a Stirred-Flow Reaction Chamber. Soil Sci. Soc. Am. J. 53, 406–410. https://doi.org/10.2136/sssaj1989.03615995005300020016x

Silva, S.H.G., Silva, E.A., Poggere, G.C., Junior, A.L.P., Gonçalves, M.G.M., Guilherme, L.R.G., Curi, N., 2020. Modeling and prediction of sulfuric acid digestion analyses data from pxrf spectrometry. Sci. Agric. 77. https://doi.org/10.1590/1678-992x-2018-0132

Smil, V., 2000. Phosphorus in the Environment: Natural Flows and Human Interferences. Annu. Rev. Energy Environ. 25, 53–88. https://doi.org/10.1146/annurev.energy.25.1.53

Smolders, E., Nawara, S., De Cooman, E., Merckx, R., Martens, S., Elsen, A., Odeurs, W., Vandendriessche, H., Santner, J., Amery, F., 2021. The phosphate desorption rate in soil limits phosphorus bioavailability to crops. Eur. J. Soil Sci. 72, 221–233. https://doi.org/10.1111/ejss.12978

Sun, W., Roy, A., Selim, H.M., 2019. Residence time effects on molybdenum adsorption on soils: Elucidation by multi-reaction modeling and xanes analysis. Soil Syst. 3, 1–14. https://doi.org/10.3390/soilsystems3030055

Sun, W., Selim, H.M., 2019. A general stirred-flow model for time-dependent adsorption and desorption of heavy metal in soils. Geoderma. https://doi.org/10.1016/j.geoderma.2019.03.034

Tavares, C.A., Santos, T.M.R., Lemes, N.H.T., dos Santos, J.P.C., Ferreira, J.C., Braga, J.P., 2020. Solving ill-posed problems faster using fractional-order Hopfield neural network. J. Comput. Appl. Math. 381, 112984. https://doi.org/10.1016/j.cam.2020.112984

Torrent, J., 1991. Activation energy of the slow reaction between phosphate and goethites of different morphology. Aust. J. Soil Res. 29, 69–74. https://doi.org/10.1071/SR9910069

Torrent, J., Barron, V., Schwertmann, U., 1990. Phosphate adsorption and desorption by goethites differing in crystal morphology. Soil Sci. Soc. Am. J. 54, 1007–1012.

Vance, C.P., Uhde-Stone, C., Allan, D.L., 2003. Phosphorus acquisition and use: Critical adaptations by plants for securing a nonrenewable resource. New Phytol. 157, 423–447. https://doi.org/10.1046/j.1469-8137.2003.00695.x

Wang, L., Putnis, C. V., Hövelmann, J., Putnis, A., 2018. Interfacial precipitation of phosphate on

hematite and goethite. Minerals 8, 207. https://doi.org/10.3390/min8050207

Wang, X., Hu, Y., Tang, Y., Yang, P., Feng, X., Xu, W., Zhu, M., 2017. Phosphate and phytate adsorption and precipitation on ferrihydrite surfaces. Environ. Sci. Nano 4, 2193–2204. https://doi.org/10.1039/c7en00705a

Wang, X., Phillips, B., Boily, J.-F., Hu, Y., Hu, Z., Yang, P., Feng, X., Xu, W., Zhu, M., 2019. Phosphate Sorption Speciation and Precipitation Mechanisms on Amorphous Aluminum Hydroxide. Soil Syst. 3, 20. https://doi.org/10.3390/soilsystems3010020

Warrinnier, R., Goossens, T., Braun, S., Gustafsson, J.P., Smolders, E., 2018. Modelling heterogeneous phosphate sorption kinetics on iron oxyhydroxides and soil with a continuous distribution approach. Eur. J. Soil Sci. 69, 475–487. https://doi.org/10.1111/ejss.12549

Wen, Y., Wen, J., Wang, Q., Bai, L., Wang, Y., Su, S., Wu, C., Zeng, X., 2021. Organic carbon preservation promoted by aromatic compound-iron complexes through manure fertilization in red soil. J. Soils Sediments 21, 295–306. https://doi.org/10.1007/s11368-020-02769-y

Withers, P.J.A., Sylvester-Bradley, R., Jones, D.L., Healey, J.R., Talboys, P.J., 2014. Feed the Crop Not the Soil: Rethinking Phosphorus Management in the Food Chain. Environ. Sci. Technol. 48, 6523–6530. https://doi.org/10.1021/es501670j

Yin, Y., Allen, H.E., Huang, C.P., Sparks, D.L., Sanders, P.F., 1997. Kinetics of mercury(II) adsorption and desorption on soil. Environ. Sci. Technol. 31, 496–503. https://doi.org/10.1021/es9603214

Zhang, T., Lu, Y., Luo, G., 2017. Effects of temperature and phosphoric acid addition on the solubility of iron phosphate dihydrate in aqueous solutions. Chinese J. Chem. Eng. 25, 211–215. https://doi.org/10.1016/j.cjche.2016.06.009